
UCL DEPARTMENT OF GEOGRAPHY



Seagrass Mapping's Efficiency: A comparative analysis
of high-resolution orthoimages and Sentinel-2 imagery
in Gökova Bay, Turkey

GJJB4

University College London (UCL)
Department of Geography

Supervisor: Mathias Disney

2024

UCL DEPARTMENT OF GEOGRAPHY



DEPARTMENT OF GEOGRAPHY
BA/BSc Geography

Please complete the following declaration and include this form after the title sheet of your dissertation.

I, GJJB4, hereby declare:

- a. that this dissertation is my own original work and that the exact source of any material (ideas, information, figures or text) derived or quoted from the published or unpublished work of other persons has been cited according to the required conventions
- a. that I have read the UCL Academic Integrity policy on plagiarism, self-plagiarism, collusion, falsification and contract cheating
- a. that the dissertation has been prepared specially for the BA/BSc in Geography of UCL (University College London);
- a. that the dissertation does not contain any material previously submitted to the examiners of this or any other University, or any material previously submitted for any other examination.

Number of words: 7325

Signed: GJJB4

Date: 16/03/2024.....

Please note that the Department of Geography makes dissertations available online for consultation by other students and staff. They cannot be downloaded. If you wish your dissertation to be excluded from those made available for others to view, please send an email to the relevant dissertation convenor, with a copy to Nick Mann.

For further details about how UCL processes your personal data, please see the [UCL Student Privacy Notice](#).

Abstract

Seagrass meadows are essential carbon sinks, capturing carbon thirty-fives times faster than tropical forests. They play a fundamental role in mitigating environmental change. This study focuses on the distribution of these habitats in Gökova Bay, Turkey. This is done using high-resolution imagery and freely-accessible Sentinel-2 satellite data. The softwares used to achieve this are QGIS and Google Earth Engine. Ground-truth data is used to validate the maps and assess the accuracy of the model. These species offer breeding grounds and nursery to other marine biodiversity. They also capture carbon through the biogeochemical process of photosynthesis, thereby becoming essential habitats in carbon-offsetting and contributing to the blue carbon market. The ecological services that these ecosystems provide make them crucial in stabilising the marine food webs. From a broader perspective, through the evaluation of different methodologies and their outcomes, this research aims to assist with monitoring strategies.

Acknowledgments

Firstly, I would like to thank my supervisors, Mathias Disney and Harry Heorton, for their unprecedented guidance throughout this dissertation. I would like to express my gratitude towards Zafer Kızılkaya for introducing PlanBlue to me. From PlanBlue, I would like to thank Svenja Diester and Anna-Lea Lesage for providing their data to me, after asking for their assistance to such an extent. Without their help this would have not been possible. I feel sincere appreciation for my boss at KlimateNet, Anne-France Kennedy, who first exposed me to blue carbon projects and has supported me throughout this dissertation. I would also like to thank my mother and Romain Lautard who took time to support me with the technical parts of this project. Finally, my father, who inspires me every day to make meaningful change.

Table of Contents

Abstract	ii
Acknowledgements	iii
List of Figures and Tables	
List of Acronyms	
Preface	iv
1. Introduction	1
1.1 Seagrass Systems	1
1.2 <i>P. oceanica</i> in Comparison to Other <i>Posidonia</i> Species	2
1.3 Threats to Seagrasses	3
1.4 Research on Anthropogenic Impacts on Seagrasses	4
1.5 Value of Ecosystem	5
1.6 Need for Conservation	6
1.7 Ongoing Restoration and Monitoring Efforts	7
1.8 Remote Sensing as a Tool of Monitoring	8
1.9 Previous RS Studies	9
2. Aims & Research Questions	10
3. Study Site	11
4. Methods	12
4.1 Data Acquisition	12
4.2 Orthoimages Processing	13
4.3 Threshold-based Classification Using QGIS	14
4.4 Validation and Error Analysis	15
4.5 Statistical Analysis	16
4.6 Sentinel-2 Imagery Processing	17
4.7 Classification	18
4.8 Pixel Size Comparison	19
5. Results	20
5.1 Orthoimages and Ground-truthing	20
5.2 Classification Results and Accuracy Assessment	21

5.3 The European Atlas of the Seas and Sentinel-2	22
5.4 S-2 Classification Results Compared with Orthoimages' Classification	23
5.5 Accuracy Assessment at Reduced Resolution for the Orthoimage	24
6. Discussion	25
6.1 Orthoimage Classification and Accuracy	25
6.2 High-resolution Data Limitations	26
6.3 Software Limitations and Threshold-based Approach	27
6.4 Comparative Analysis with S-2 Data	28
6.6 Broader Implications of Findings	29
Conclusion	30
Appendice.....	
Appendix 1. Orthoimage Classification and Accuracy	

List of Figures and Tables

Fig. 1: *Posidonia oceanica* meadows in their natural habitat (A); a plant of *P. oceanica* with four plant parts (B). (Poli et al., 2020)

Fig. 2: Seagrass species sequester carbon in different ways: a) larger and more structurally complex seagrasses lead to higher input of organic matter, resulting in higher accumulation of biomass. More efficient burial and long-term storage of CO₂ make the species an important carbon sink. *P. oceanica* is one of those species. b) Smaller, less structurally complex seagrass species exist, and result in lower biomass accumulation as well as less efficient burial of CO₂. Less effective carbon sinks. (Simpson et al., 2022).

Fig. 3: Through its rhizomes, seagrasses are fixed to the substrate and keep the sediment immobile. In addition, they play an important role in the beach-dune dynamic, since the *Posidonia* meadows are a sediment reservoir which feed the beaches and dunes. (Med Posidonia Network 2023)

Fig. 4: Framework on marine ecosystems' role in carbon cycling. From left to right: when ecosystems are defined as carbon sink or source, the water depth, depositional environment and sediment matrix are analysed to distinguish C_{org} and C_{inorg} . These carbon stocks are represented spatially, with the red area showing the carbon source (due to human activities or natural processes) and the green area showing carbon sink, helping to offset atmospheric carbon dioxide (Monnier et al., 2022).

Fig. 5: Transplanted seedlings at Elba Island, Italy (top image).
Transplants at set-up (A) and a year later (B). (Piazzi et al., 2021)

Fig. 6: Top: Every orthoimage's location in Gökova Bay. Bottom: zoomed on the 6th orthoimage (post-classification) (see Fig. 15 for close-up image).

Fig. 7: Example of a sand patch from orthoimage 1

Fig. 8: Top: Validation orthoimage displayed on QGIS. Bottom: ground-truth data polygons with values (0 or 1) assigned for each class (seagrass / non-seagrass).

Fig. 9: Stages of the validation orthoimage's classification and comparison between unsupervised and supervised classifications. Top: Ground-truth validation polygons, green represents seagrass, yellow represents sand. Middle: Unsupervised classification. Bottom: Supervised classification.

Fig. 10: Flowchart of the data acquisition and processing steps for orthoimages

Fig. 11: Top: Syros Island on a map. Bottom: The European Atlas of the Seas by EMODNet showing *P. oceanica*' distribution around Syros Island. Legend shows seagrass distribution from absent 0 (blue) to present 1 (red).

Fig. 12: Grayscale map of Syros Island, white representing land and grey water, green polygons can be spotted along the shores, representing seagrasses. Zoomed into the satellite imagery, with polygons differentiating seagrass (green) from non-seagrass (yellow) drawn through comparison with the European Atlas of the Seas' pixels.

Fig. 13: Flow chart for Sentinel-2 methodology

Fig 14: Band values identified using the 'Select Feature' tool on QGIS for the sand patch in Fig., for each orthoimage and on an 8-bit scale

Fig. 15: Display of classified (left) and unclassified (right) orthoimages. Black: seagrass, Yellow: sand.

Fig. 16: Top: Classified orthoimage 4. Middle: Orthoimage 4 anomalies. 'Malfunction Gap' indicates a section where imaging was not captured due to potential camera malfunction. 'Shadowing' refers to areas where the camera casts shadows. Bottom: Orthoimage 6 anomalies. 'Imaging error' identifies the unintentional inclusion of a diver in the imagery.

Fig. 17: Seagrass coverage shown as a percentage of the total area (in m²) for each orthoimage

Fig. 18: Map of Syros Island generated on GEE after the binary classification process. Red: seagrass, Green: non-seagrass.

Fig. 19: Top: Overlay of the validation orthoimage on S-2 imagery, pixels outlined. Bottom: Overlay of S-2 imagery on the validation orthoimage, pixels outlined.

Fig. 20: Frequency distributions of pixel values for every band of the orthoimage and S-2

Fig. 21: Downscaling validation orthoimage's resolution at 10 metre-per pixel (a), at 1 metre-per pixel (b), at 0.5 metre-per pixel (c), at 0.05 metre-per pixel (d).

Fig. 22: A close-up view of a seagrass patch taken from the validation orthoimage until pixels are clear.

Fig. 23: Example of hyperspectral camera called DiveRay used by PlanBlue at Finger Reef (Mills et al., 2023).

Table 1: The economic value of *P. oceanica*'s ecosystem services in 1990 and 2006 (Vassallo et al., 2013).

Table 2: Band values identified using the 'Select Feature' tool on QGIS for the sand patch in Fig. 7

Table 3: Averages of band values identified on QGIS for the two classes and for each orthoimage (8-bit scale)

Table 4: Total area of each orthoimage (in m²)

Table 5: The validation orthoimage's error matrix

Acronyms

BC - Blue Carbon

P. - *Posidonia*

C_{org} - Organic carbon

C_{inorg} - Inorganic carbon

EMODNet - European Marine Observation and Data Network

GEE - Google Earth Engine

MCS - Marine Conservation Society

ROI - Region of Interest

RS - Remote Sensing

MPA - Marine Protected Area

S-2 - Sentinel-2

RF - Random Forest

TP - True Positive

FN - False Negative

SVM - Support Vector Machine

Preface

Growing up in the Mediterranean, and more precisely along the Aegean Sea, my initial encounters with seagrasses were far from appreciative. Like many, I found sand more appealing than seagrasses while swimming. However, this perception changed the moment I started scuba diving. I discovered the striking role the endemic species of *Posidonia oceanica* plays in the Mediterranean and on a global scale, not only as a thriving ecosystem crucial for this sea, but also as a key carbon stock.

My journey into blue carbon began with my role at Klimatenet, a startup led by a visionary who deeply values the conservation of these ecosystems. This experience not only broadened my understanding but also solidified my interest in becoming a blue carbon facilitator. I found myself engaging with remote sensing experts, striving to map these ecosystems. Taking the module of remote sensing in my second year of my undergraduate directed my academic path towards satellite technology.

Attending the Whitley Fund for Nature's summit in London in November 2023, I had the opportunity to engage in a conversation with Zafer Kızılkaya, founder of the Mediterranean Conservation Society. Mr. Kızılkaya shared insights on PlanBlue's technology, explaining the high mapping accuracy for seagrasses in their study sites in Turkey. Following this, I reached out to PlanBlue and they generously shared their data with me.

This dissertation's objective is to demonstrate that through the application of appropriate tools and methodologies, accurate mapping and monitoring of seagrass meadows are achievable. I aspire for my research to serve as a replicable model, adaptable across various regions over time to observe the evolution of seagrass beds.

1. Introduction

1.1 Seagrass systems

Blue carbon (BC) is a concept which refers to the ability of underwater environments to sequester carbon dioxide from water (Pergent-Martini et al., 2021). Among these ecosystems, seagrass meadows are extremely valuable, sequestering carbon thirty-five times faster than tropical forests (Neufeld 2024) (Topouzelis et al., 2018). These habitats are located in temperate climates, in the middle latitudes, including North Atlantic and Pacific Oceans. This study focuses on the Mediterranean Sea, and more specifically Gökova Bay in the Aegean Sea (Traganos et al., 2018). Globally speaking, seagrass species are not as diverse as other marine species, with only sixty-four known in the world (Pergent-Martini et al., 2021).

In the Aegean Sea, the species of *Posidonia oceanica*, *Cymodocea nodosa* and *Zostera noltii* are the most abundant. Often referred to as ‘the lung of the seas’, *P. oceanica*, an endemic species to the Mediterranean, is known as the most productive at carbon fixation, and thrives particularly in Gökova Bay, Turkey (Fig. 6) (Duman et al., 2019). The species lives in temperatures between 11°C and 29°C, in saline waters where salinity does not exceed 38.5 psu and clear waters at depths of 0-40m (Sánchez-Lizaso et al., 2007) (Akçalı & Cirik 2015). Carbon sequestration varies depending on seagrass structure, with *P. oceanica* efficiently storing carbon through its large canopy, in contrast to smaller and simpler species (Fig. 2) (Simpson et al., 2022). The parameters needed for *P. oceanica* to thrive in these locations are physical (salinity, waves, temperature) and natural phenomena related to photosynthetic productivity (light availability, nutrient levels, disease prevalence) (Short et al., 2001) (Fig. 2). In the Mediterranean Sea, clear waters facilitate deep light penetration, reaching depths of up to forty-five metres, which coincide with the maximum depth of the species (Duman et al., 2019) (Fornes et al., 2006). However, at depths of forty metres, there is a significant reduction of light, affecting the plant’s primary productivity (Monnier et al., 2022). Nutrients in the water (phosphates and nitrates) are fundamental for photosynthesis and the proliferation of the seagrass meadows (Pergent et al., 2014). Although the Mediterranean Sea is an oligotrophic (nutrient-poor) environment, *P. oceanica* compensates with its extensive root system, extracting nutrients from the sediment (Fig. 1) (Fig. 2)

(Pergent et al., 2014). This sedimentary role of the species is also critical for the wider coastal ecosystems, as *P. oceanica* helps to maintain shoreline stability and prevent erosion (Fig. 3) (Med Posidonia Network 2023).

Unlike plants on land, seagrasses lack stomata, the pores on plants' leaves controlling water and gas exchange. Yet, they possess a cuticle layer which makes this exchange. The oldest known plant is a clone of *P. oceanica*, which is estimated to be 200,000 years old, from the ice ages of the late Pleistocene (Reynolds 2018). The resilience of this species comes from its shoots, capable of surviving for over three decades (Reynolds 2018). These shoots originate from rhizomes and grow horizontally by a few centimetres annually (Fig. 1) (Duman et al., 2019). Through the accumulation of rhizomes, dense matted form over time, becoming reef-like structures (Fig. 1) (Duman et al., 2019).

These complex structures stabilise sediments and dissipate wave energy, reducing water turbidity and protecting shorelines from erosion (Fig. 2) (Fig. 3) (Duman et al., 2019). *P. oceanica*'s role aligns with the UN Sustainability Goals, particularly SDG 14 -- Life Below Water -- focusing on sustainably using ocean resources (Neufeld 2024).



Fig. 1: *Posidonia oceanica* meadows in their natural habitat (A); a plant of *P. oceanica* with four plant parts (B). (Poli et al., 2020).

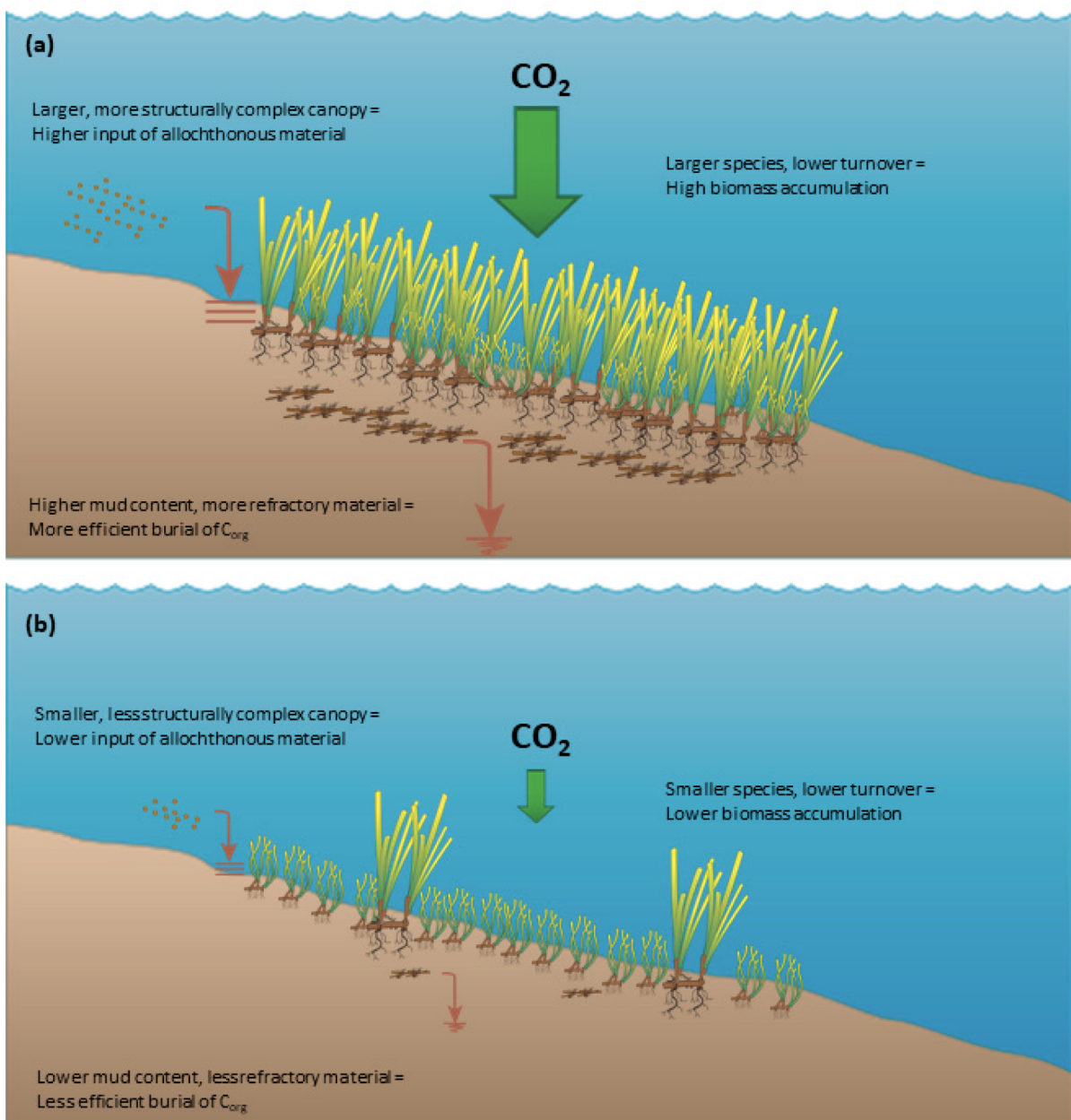


Fig. 2: Seagrass species sequester carbon in different ways: a) larger and more structurally complex seagrasses lead to higher input of organic matter, resulting in higher accumulation of biomass. More efficient burial and long-term storage of CO_2 make the species an important carbon sink. *P. oceanica* is one of those species. b) Smaller, less structurally complex seagrass species exist, and result in lower biomass accumulation as well as less efficient burial of CO_2 . Less effective carbon sinks. (Simpson et al., 2022).

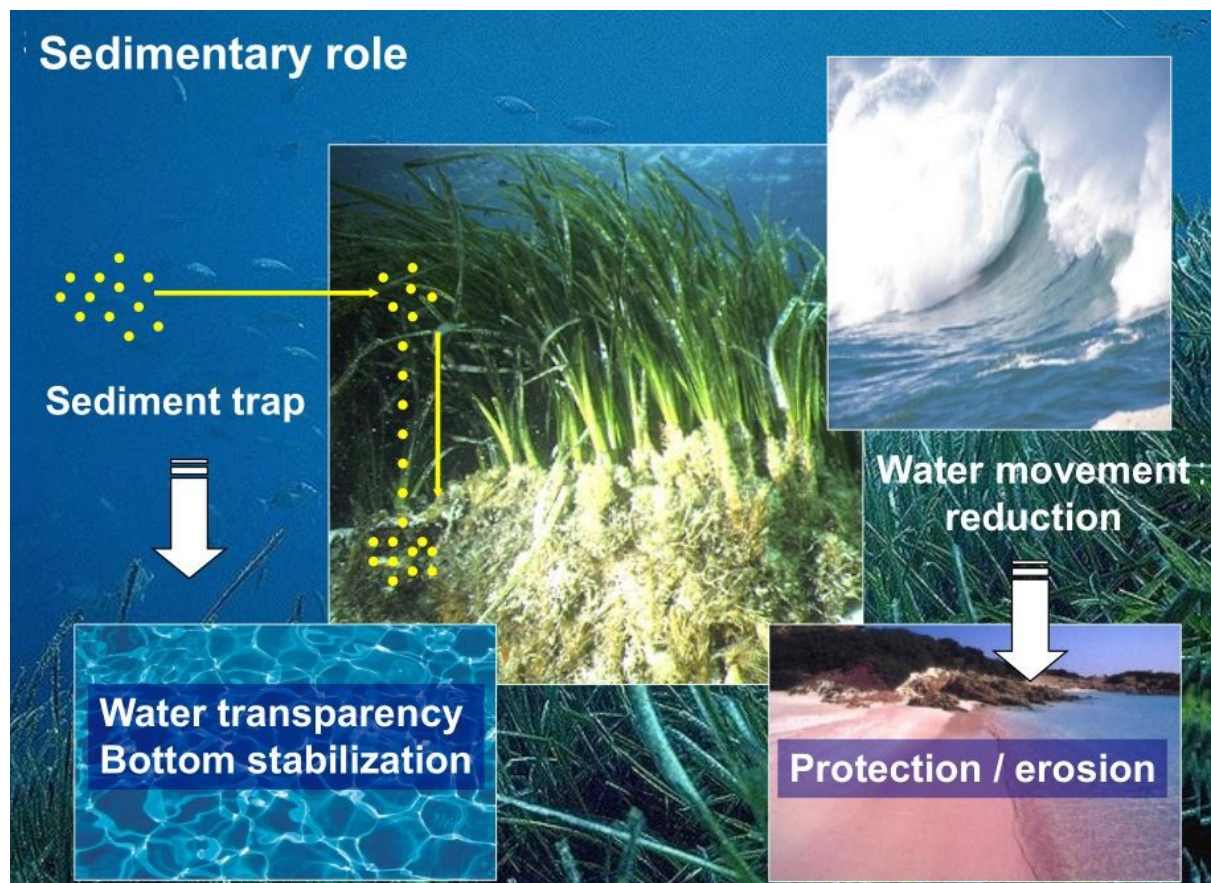


Fig. 3: Through its rhizomes, seagrasses are fixed to the substrate and keep the sediment immobile. In addition, they play an important role in the beach-dune dynamic, since the *Posidonia* meadows are a sediment reservoir which feed the beaches and dunes. (Med Posidonia Network 2023)

1.2 *P. oceanica* in comparison to other *Posidonia* species

Literature shows that *P. oceanica* meadows possess significantly deeper levels of organic sediment compared to other *Posidonia* species such as *Posidonia australis*, found in Australia. *P. oceanica*'s can be found at depths up to forty-five metres, but on average are found at eight metres, while *P. australis* reaches 2.5 metres, with vertically growing rhizomes (Fig. 1) (Lavery et al., 2013). Consequently, *P. oceanica* holds greater quantities of sedimentary organic carbon (C_{org}) (Lavery et al., 2013). In terms of carbon storage, *P. oceanica*'s carbon stock can reach approximately 448 million tonnes per year globally, with an annual increase ranging from 0.28 to 18.4 million tonnes (Lavery et al., 2013). This result surpasses estimates for *P. australis* by tripling them, and even exceeds Australia's annual CO₂ emissions by more than 300% (Lavery et al., 2013).

This comparison deepens the understanding of the differences in carbon storage capacity among various seagrass species. Nellemann et al. (2009) have emphasised the importance of considering variations between different marine habitats when estimating BC stocks. Neglecting these distinctions could oversimplify matters and introduce discrepancies in estimates (Nellemann et al., 2009).

1.3 Threats to seagrasses

Highly sensitive to the increase and variation of lights, salinity, sedimentation and turbidity, *P. oceanica* are becoming extremely vulnerable at locations with high human activity, such as boat anchoring and trawling (Pergent et la., 2016). The species' vulnerability is further emphasised by its listing on the Red List of threatened species (Boudouresque et al., 2006). A direct indication of physical damage on seagrasses are scars formed by these human practices.

Marine pollution occurs due to urban waste and agricultural activities (nutrient runoff and the use of organic pollutants), posing a great threat to seagrass habitats (Marbá and Duarte 2010). These activities also lead to the emergence of the invasive species *Caulerpa taxifolia* and *Caulerpa cylindracea*, living on the rhizomes of *P. oceanica* and causing great damage to the meadows (Fig. 1) (Marbá and Duarte 2010).

1.4 Research on Anthropogenic impacts on seagrasses

Seagrass meadows' biggest threats are human activities. Okus et al. (2010) conducted a research in Gökova Bay, where they examined anchor-induced damage on *P. oceanica* along a 220 km stretch of the coastline (Okus et al., 2010). They revealed that 61% of these meadows are affected by anchoring and trawling (fishing) activities (Okus et al., 2010). The dropping and dragging of anchors disrupt the seafloor and the bed structure, and can also uproot seagrass shoots (Boudouresque et al., 2009). Several Mediterranean nations have implemented regulations to prevent trawling near the coast, with countries like Tunisia, Italy and France enforcing laws to ban trawling within three nautical miles from the shoreline (Boudouresque et al., 2009). While Boudouresque et al. (2009) evaluate trawling as the most

impactful human activity to these ecosystems, other significant threats exist. Duman et al. (2019) identify the development of urban and harbour infrastructures, as well as sand extraction and seawalls as primary influences affecting the growth of seagrass meadows. Research by Koçak et al. (2007) assessed copper and zinc contamination in sediments and *P. oceanica* around a fish farm in the Aegean Sea, suggesting that shoot density, leaf length and area decrease significantly with this contamination. Additionally, a recent study by Pansini et al. (2022) discusses how escalated sedimentation rates and nutrient loading are major disruptors to these marine habitats.

Duman et al., (2019) combined acoustic technology, sedimentological, oceanographic, geomorphological data and aquatic video cameras to understand *P. oceanica*'s distribution in Turkey's western coasts. They discovered that *P. oceanica* are also receding at locations without human impact, suggesting climate change has an influence on the species (Duman et al., 2019). Ocean warming, sea level rise and increasing extreme weather events highly damage these ecosystems (Pergent et al., 2016). It is also important to note that the species has limited genetic diversity and a slow growing rate, meaning that once these disturbances occur, the recovery capacity diminishes (Boudouresque et al., 2009).

1.5 Value of ecosystem

P. oceanica has an indirect role in benefitting society and economy (Vassallo et al., 2013). Assigning economic value to ecosystems influences both public and private sectors to adopt sustainable practices. The Millennium Ecosystem Assessment lists the services given by the carbon sink *P. oceanica* as providing breeding grounds for other species, creating high biological productivity zones, stabilising sediments and acting as food sources for other organisms (Hein et al., 2006). There is a lack of research on the global monetary value of these habitats, however research conducted on the Marine Protected Area of the Isle of Bergeggi in Italy is an exemplary case of how these ecosystems can be quantified (Vassallo et al., 2013). The calculation of input flows (ecological services) on one m² of *P. oceanica* has been estimated to be a total of 2,240€ per m² annually (Blasi 2009). The value of the species in maintaining other coastal ecosystems has been estimated to be 0.8€ per m² annually (Blasi 2009).

In 1990, living *P. oceanica*'s global extent was 260,000 m² and the economic value was 44,800,000€ annually (Table 1) (Vassallo et al., 2013). In 2006, the extent decreased to 140,000 square metres and the economic value to 24,100,000€ annually (Table 1) (Vassallo et al., 2013). Physically speaking, the species declined by 120,000 m², which led to a decrease in the value of the provided ecosystem services, by 20,700,000€ per year, due to important threats on the ecosystems (Table 1) (Vassallo et al., 2013).

Table 1: The economic value of *P. oceanica*'s ecosystem services in 1990 and 2006 (Vassallo et al., 2013).

Year	Living <i>P. oceanica</i> extent (m²)	Economy value (€a⁻¹)
1990	2.60E+05	4.48E+07
2006	1.40E+05	2.41E+07

Over recent decades, the demand to quantify carbon sequestration capabilities of marine environments has increased significantly, with the urgent need to decrease atmospheric carbon dioxide levels (Monnier et al., 2022). Seagrass meadows are capable of storing important amounts of organic carbon (C_{org}), contributing to a globally impactful carbon sink (Fig. 4) (Smith, 1981). Despite existing on a minor extent of the ocean's surface (~0.2%; 160,000–600,000 km²), seagrass ecosystems' C_{org} rates account for nearly 10–18% of total oceanic sediment carbon burial (McKenzie et al., 2020) (Duarte et al., 2005).

Quantifying C_{org} storage capacity can become an incentive for carbon-emitting entities to invest in the BC market and offset their emissions by investing in the preservation of marine ecosystems (Fig. 4). This process highlights the economic value which can be given to seagrasses and encourages the protection of their habitats through the recognition of their critical role in the broader context of sustainability.

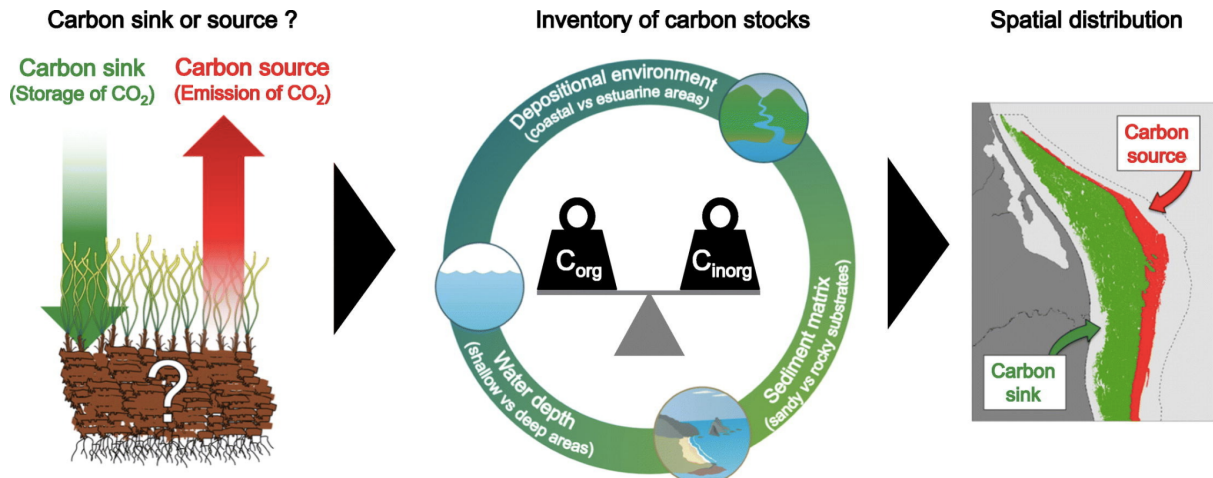


Fig. 4: Framework on marine ecosystems' role in carbon cycling. From left to right: when ecosystems are defined as carbon sink or source, the water depth, depositional environment and sediment matrix are analysed to distinguish C_{org} and C_{inorg} . These carbon stocks are represented spatially, with the red area showing the carbon source (due to human activities or natural processes) and the green area showing carbon sink, helping to offset atmospheric carbon dioxide (Monnier et al., 2022).

However, the efficiency of carbon offsetting efforts has been surrounded by criticisms since The Guardian's 2023 investigation into rainforest carbon offsets, suggesting that 90% of them are 'worthless' (Greenfield 2023). This is due to the certifiers in the market, who play a crucial role by validating the emissions reductions and carbon sequestration efforts on projects, proven not to be as substantial as previously thought (Greenfield 2023). Given its recent emergence, the BC market needs to benefit from the mistakes made by forest carbon offsetting. The establishment of a reliable, transparent framework is essential to ensure credible incentivising of seagrass preservation.

1.6 Need for conservation

Although this research only focuses across the scale of a bay, large-scale monitoring is a fundamental step for preservation. Planning ecosystem management in the whole of the Mediterranean Sea requires the acknowledgement of geopolitical and biogeographical landscapes (Appolloni et al., 2020). With twenty-one diverse nations and millions of livelihoods sustained by the region, which, itself, is located on three different continents, important disparities in socio-economic conditions appear (Appolloni et al., 2020). The collaboration between stakeholders and scientists is crucial to build cooperation and protect

vulnerable ecosystems. Systematic observation of *P. oceanica* only began in the 1980s, nevertheless, the EU has developed new legislative measures for this species today (Appolloni et al., 2020) (Akçalı & Cirik 2015). It designated it as a priority habitat under the Habitats Directive (and more specifically the Council Directive 92/43/EEC) (Appolloni et al., 2020) (Akçalı & Cirik 2015).

1.7 Ongoing restoration and monitoring efforts

At the moment, there is still a significant lack of data in the Southern and Eastern Mediterranean in contrast to the Western Mediterranean (Telesca et al., 2015). Surveillance and regular mapping is crucial to overcome this challenge. In this research, [the European Marine Observation and Data Network \(EMODnet\) Seabed Habitats platform](#) plays a pivotal role, serving as a repository for the distribution of specific species, such as *P. oceanica*, allowing the submission or retrieval of information.

There are diverse approaches to restore these habitats, including the use of metal rods to secure the meadows' shoots (Fig. 1). Piazzì et al. (2021) explored two restoration strategies to understand which would be the most effective (Piazzì et al., 2021). They consist of either using non-degradable matte or degradable ones, which had not been previously used (Piazzì et al., 2021). This new innovative technique of using a degradable matte on a deceased one showed the most efficient recovery of degraded *P. oceanica* (Fig. 5) (Piazzì et al., 2021). This simulates the plant's natural recovery by supporting its rooting of cuttings and seedlings, whilst fostering the colonisation of benthic species, allowing the restoration of the overall ecosystem (Fig. 5) (Piazzì et al., 2021). Although these are cost and time-efficient, the practical application of these methods on a larger scale would be challenging, as the success and efficiency of such habitat restoration efforts can vary significantly based on environmental conditions, the extent of degradation, and resource availability.

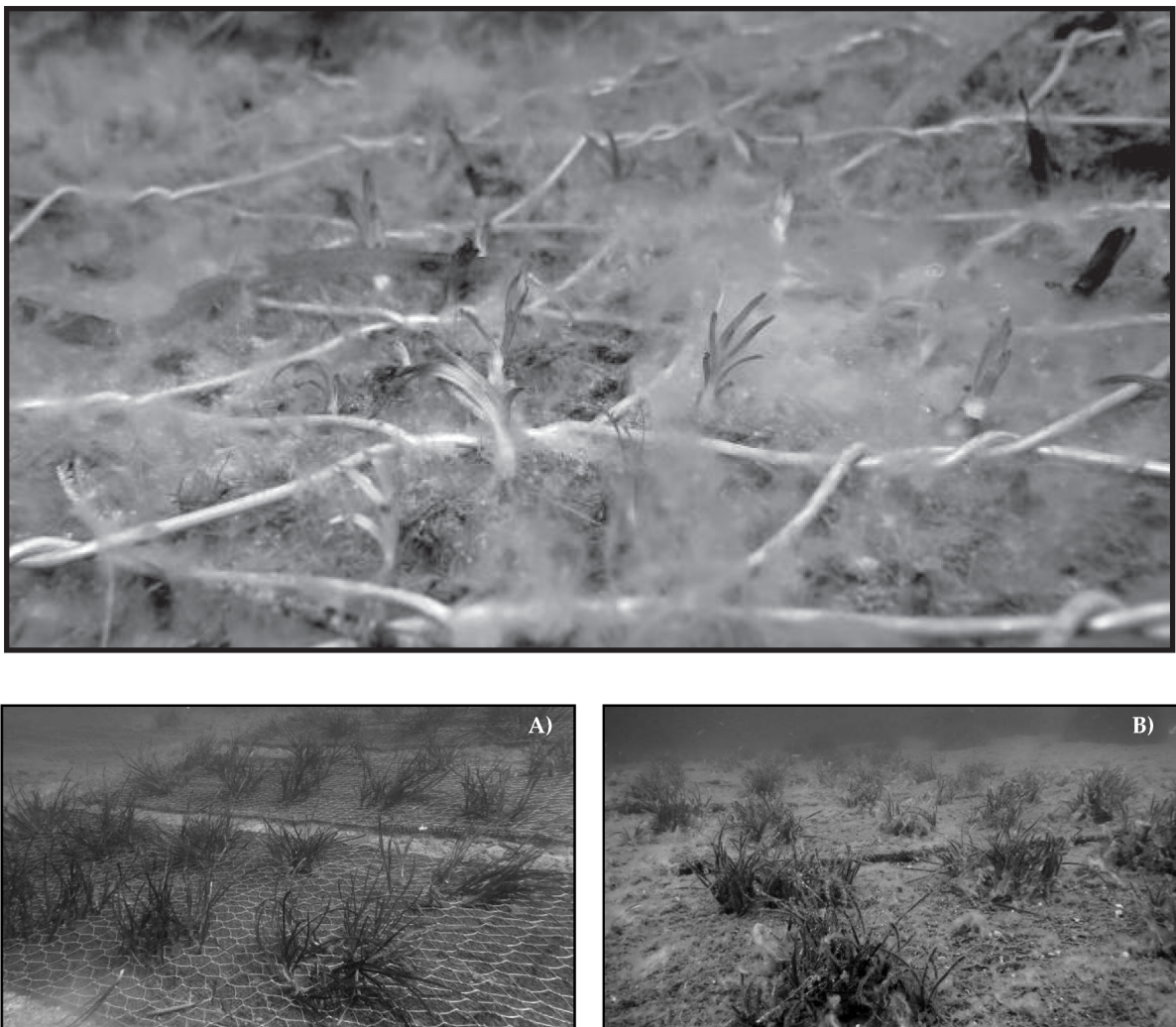


Fig. 5: Transplanted seedlings at Elba Island, Italy (top image). Transplants at set-up (A) and a year later (B). (Piazz et al., 2021)

1.8 Remote sensing as a tool of monitoring

Remote sensing (RS) can be defined as the science of acquiring information using satellite imagery to monitor land and marine environments (Mills et al., 2023). Underwater hyperspectral imaging in RS has higher benefits compared to traditional methods such as photo quadrat surveys (Mills et al., 2023). Although hyperspectral imaging requires time and effort, it is still less time-consuming and resource-intensive than traditional methods (Mills et al., 2023). After the preprocessing stages, RS can provide rapid analysis of data through existing automated processing systems (Mills et al., 2023). It reduces weeks of work required for traditional methods to just a couple of minutes to hours (Mills et al., 2023). This shows

the long-term savings of choosing RS over other methods, contributing to large-scale monitoring efforts (Mills et al., 2023).

The use of RS expands to include the management of Marine Protected Areas (MPAs), which aim to preserve marine ecosystems and mitigate the effects of human impacts (Mills et al., 2023). Consequently, there is a growing demand for access to high-resolution RS imagery to enhance the monitoring of marine ecosystems (Mills et al., 2023). In this context, ground-truth in-situ data collection plays a vital role as well. By performing direct measurements at specific locations, the real-world reference ensures precise comparisons between observed satellite imagery and actual conditions on the ground. This significantly enhances the effectiveness of RS in the management and conservation efforts (Mills et al., 2013).

1.9 Previous RS studies

In previous studies in Greece, Traganos et al. (2018) used Sentinel-2 (S-2) imagery and ground-truth in-situ data in Thermaikos Gulf. The accuracy assessment was done through an independent validation dataset, and the overall accuracy was 72% (Traganaos et al., 2018). Similarly, Topouzelis et al. (2018) used Landsat-8 and Natura 2000 data to create a large-scale seagrass map along the Greek coast. They reported a total accuracy of 76%. Poursanidis et al. (2019) examined S-2's coastal aerosol band in three sites, including Schinias and Gavdos. Just like Topouzelis et al. (2018), they used ground-truth in-situ data and interpreted high-resolution aerial images (1m/pixel). In Schinias, the machine learning algorithm of Support Vector Machine (SVM) achieved an accuracy of 87% (Poursanidis et al., 2019). In Gavdos, a lower accuracy of 58.18% was found, due to fragmented habitats in the location (Poursanidis et al., 2019). In Bakırman & Gümüşay (2020)'s study along Gökova Bay in Turkey, machine learning algorithms were trained and accuracy assessments performed using in-situ data. The distribution of seagrass was generated with WorldView-2 satellite imagery, using both Random Forest (RF) and SVM methods. RF achieved a high accuracy (94%), while SVM demonstrated a substantial accuracy (72%). Thus, RF was determined as the best algorithm for this study (Bakırman & Gümüşay 2020).

2. Aims and Research questions

The objective of this research is to conduct a comprehensive assessment of seagrass distribution in the Gökova Bay, Turkey, aimed at informing conservation efforts. The research will use high-resolution orthoimages (geometrically corrected satellite imagery) generously provided by PlanBlue, coupled with data from the European Space Agency's Sentinel-2 (S-2) satellite missions.

This will be achieved through the following objectives:

- i. Process high-resolution orthoimages and map seagrass distributions through classification on GEE using ground-truth data extracted from QGIS.
- ii. Assess the accuracy of the distribution.
- iii. Select Sentinel-2 data on Google Earth Engine to perform a classification using the European Atlas of the Seas.
- iv. Assess the impact of image resolution on the accuracy of seagrass mapping.
- v. Evaluate the implications of mapped seagrass distributions for conservation and management.

Understanding the distribution of seagrass is essential for recognising the ecosystem's role in mitigating climate change through carbon sequestration. This knowledge is fundamental to come up with effective conservation and management strategies.

3. Study site

The Aegean Sea is located between 41°- 35° north latitude and 23°- 27°/28° east longitude, with a length of approximately 660 km, covering 214,000 km² (Fig. 6) (Kurt & Öztürk 2022). Considering morphological features, the Aegean Sea can be divided into three: the North Aegean, Middle Aegean and South Aegean (Kurt & Öztürk 2022). This semi-enclosed area has nearly 3,000 islands serving as a continuation of the maritime corridors linking the Black Sea with the Mediterranean (Kurt & Öztürk 2022). Compared to the Mediterranean, the Aegean Sea has a greater diversity of species, and forms vital habitats for seagrasses, notably species like *P. oceanica* (Duman et al., 2019). Gökova Bay is a very well-known Bay, as it is Turkey's first community-managed Marine Protected Area, built by The Mediterranean Conservation Society (MCS) (Fig. 6) (Mediterranean Conservation Society 2023). One of the primary challenges with MPAs is that once they are established, there is often limited funding and personnel available for enforcement (Mediterranean Conservation Society 2023). However, through innovative efforts, MCS engaged multiple stakeholders, including local government, divers, fishermen, and tourists, to actively collaborate on protecting the bay (Mediterranean Conservation Society 2023).



Fig. 6: Top: Every orthoimage's location in Gökova Bay. Bottom: zoomed on the 6th orthoimage (post-classification) (see Fig. 15 for close-up image).

4. Methods

4.1 Data Acquisition

This study's methodology consists of a comprehensive spatial analysis using Sentinel-2 satellite imagery and high resolution orthoimages on Google Earth Engine (GEE) to map seagrass ecosystems. The data used in this research is provided by the underwater hyperspectral imaging company, PlanBlue. This company's goal is to provide a detailed map of the seafloor and enhance understanding of marine habitats. The data includes orthoimagery with detailed metadata, specific coordinate information, pixel information and bands used. These data were initially acquired for a collaboration with the MCS.

The high-resolution orthoimages of the seafloor were captured using advanced underwater imaging techniques with specific sensors, and were operated by PlanBlue's divers as their depths vary between 24 and 29 metres, except for two of them at shallower depths (9 to 10 metres). There are six orthoimages, acquired from the 25th to 28th of May 2023.

The orthoimages have already been processed by PlanBlue, using white balancing to remove the blue hue and providing a clearer representation of the seafloor's colours for visualisation.

The primary software used is GEE, a cloud-based platform with access to an extensive archive of multi-petabyte satellite imagery. This platform, as described by Gorelick et al. (2017), facilitates high-performance computing resources essential for processing large-scale spatial datasets.

4.2 Orthoimages processing

First, it is crucial to note that the orthoimage method in this section was applied to each of the five orthoimages used as training data, with slight modification in terms of pixel values, coordinates and image asset ID. The GEE project is used to calculate the image extent (pixel size calculated using metadata).

4.3 Threshold-based classification using QGIS

The orthoimage was displayed on QGIS as a raster layer. Two classes were created, with the value of 1 assigned to seagrass and 0 to non-seagrass. Using the ‘Select Feature’ tool, approximately one hundred seagrass features were selected manually in the entirety of the orthoimage, and assigned the value of 1, and one hundred non-seagrass areas assigned the value of 0 (Fig. 7). The orthoimages were on an 8-bit scale and ranged from where 0 means no reflectance and 255 represents maximum reflectance. The spectral features’ values of every one of the seagrass and sand patches selected were visualised on the attribute table, and these values were averaged out for each class and band (Table 2). Using these figures, binary masks were created for each class on GEE across the specified bands: B1 (blue), B2 (green) and B3 (red) for orthoimages (Fig. 7) (Table 3). These binary masks were used to isolate areas of interest based on their spectral signatures. The reduce function ‘ee.Reducer.allNonZero()’ was used to aggregate the binary masks, ensuring that only pixels meeting all threshold conditions were classified as seagrass or sand. The training phase taught the classification algorithm to differentiate between seagrass and sand based on the threshold values.



Fig. 7: Example of a sand patch from orthoimage 1

Table 2: Band values identified using the ‘Select Feature’ tool on QGIS for the sand patch in Fig. 7

Bands	Values
Band 1	246
Band 2	247
Band 3	245

Table 3: Averages of band values identified on QGIS for the two classes and for each orthoimage (8-bit scale)

Orthoimage	Seagrass Band 1	Seagrass Band 2	Seagrass band 3	Sand Band 1	Sand Band 2	Sand Band 3
1	157.83	147.92	134.17	197.58	190.19	180.36
2	162.11	166.56	166.33	229.61	230.43	222.18
3	133.50	135.28	136.33	204.83	207.53	204.17
4	128.16	138.84	139.76	222.44	229.20	217.48
5	109.5	125.83	123.66	217.02	214.18	202.14
6	109.50	125.83	123.66	217.02	214.18	202.14

4.4 Validation and Error Analysis

The accuracy of the training phase was evaluated using ground-truth data from the validation orthoimage (Fig. 8). An unsupervised classification was done using a clustering process, where pixels were grouped based on their spectral similarities (Fig. 9). This was done through the K-Means clustering algorithm, in which each observation is assigned to the cluster with the closest mean (Moniruzzaman et al., 2019). Following the clustering process, a supervised classification was done using average threshold values derived from training images’ spectral reflectance values (Fig. 9). To evaluate the accuracy, ground-truth data polygons were drawn on QGIS (Fig. 8). The ‘sampleRegions’ function compares the classified image with the ground truth polygons, overlaying both observations (Fig. 9).

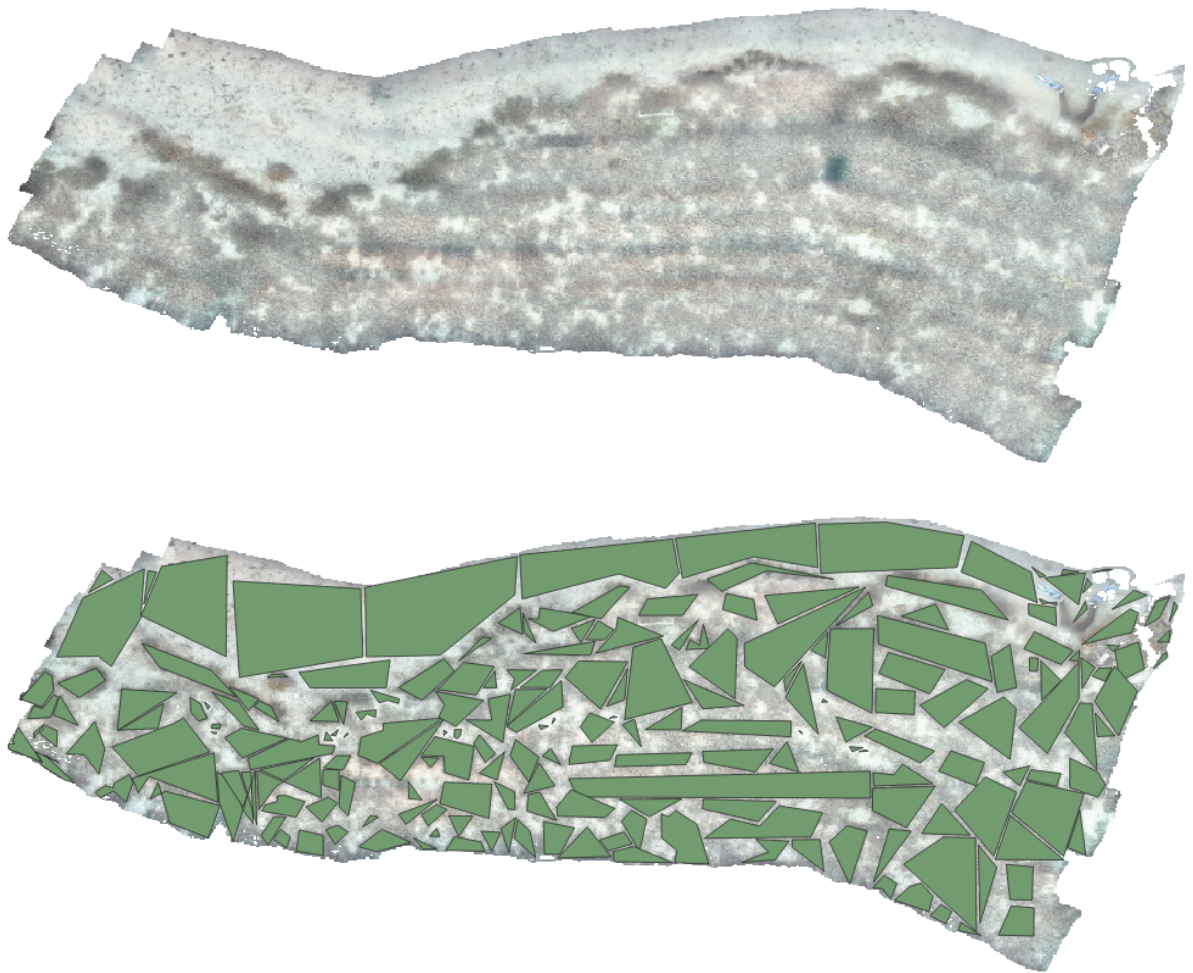


Fig. 8: Top: Validation orthoimage displayed on QGIS. Bottom: ground-truth data polygons with values (0 or 1) assigned for each class (seagrass / non-seagrass).

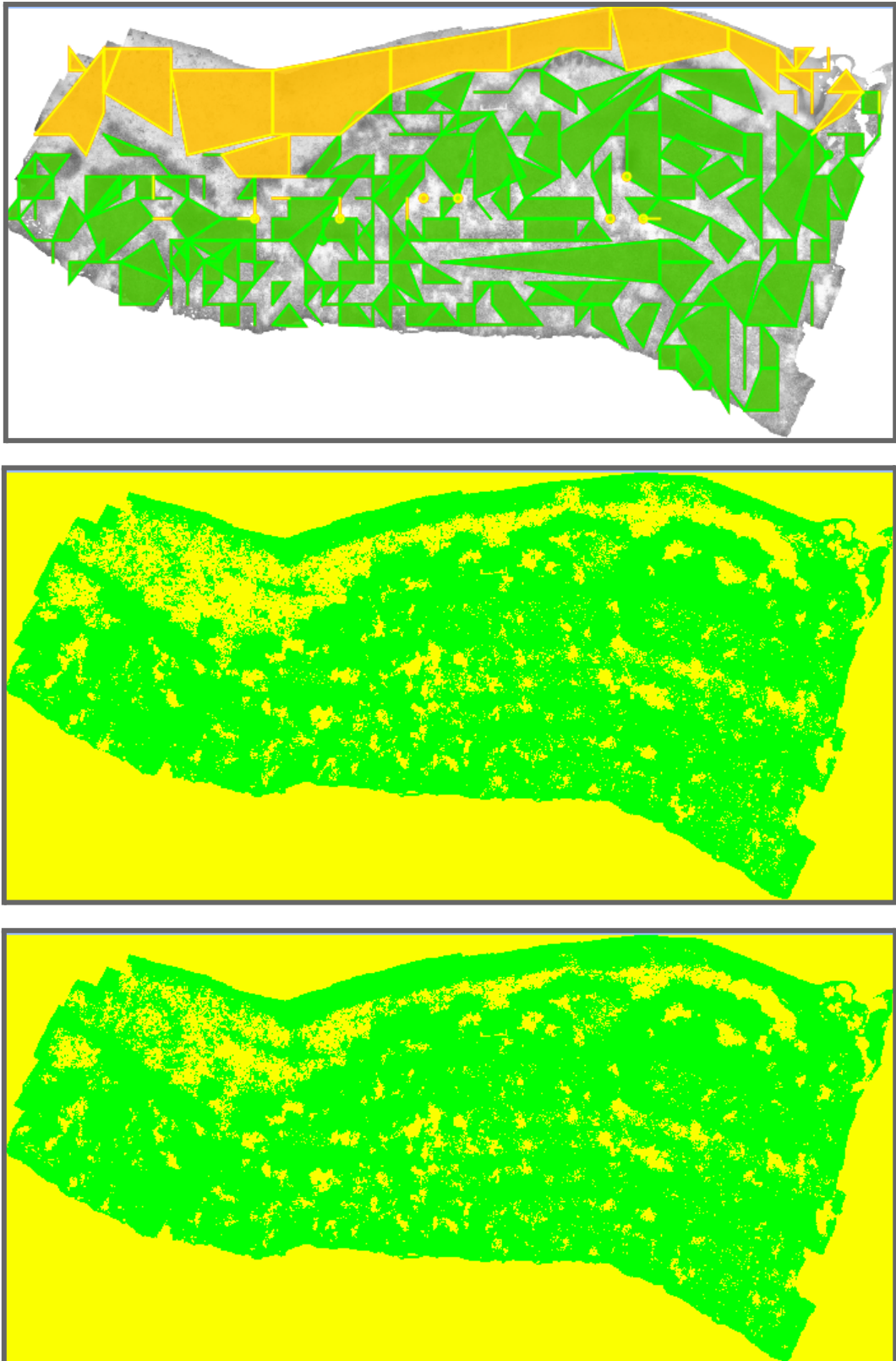


Fig. 9: Stages of the validation orthoimage's classification and comparison between unsupervised and supervised classifications. Top: Ground-truth validation polygons, green represents seagrass, yellow represents sand. Middle: Unsupervised classification. Bottom: Supervised classification.

4.5 Statistical Analysis

An error matrix was generated to assess the validation orthoimage's classification accuracy. This compared the classified values against the ground truth classes, providing metrics such as overall accuracy.

The error matrix describes the performance of the classification model. The listed values were printed on GEE. The true positives (TP) and false negatives (FN) provided by the error matrix were later on used to calculate class-specific accuracy (Gomes et al., 2020):

$$Accuracy = \frac{TP}{(TP + FN)}$$

The methods employed in this study are summarised in a comprehensive flowchart (Fig. 10).

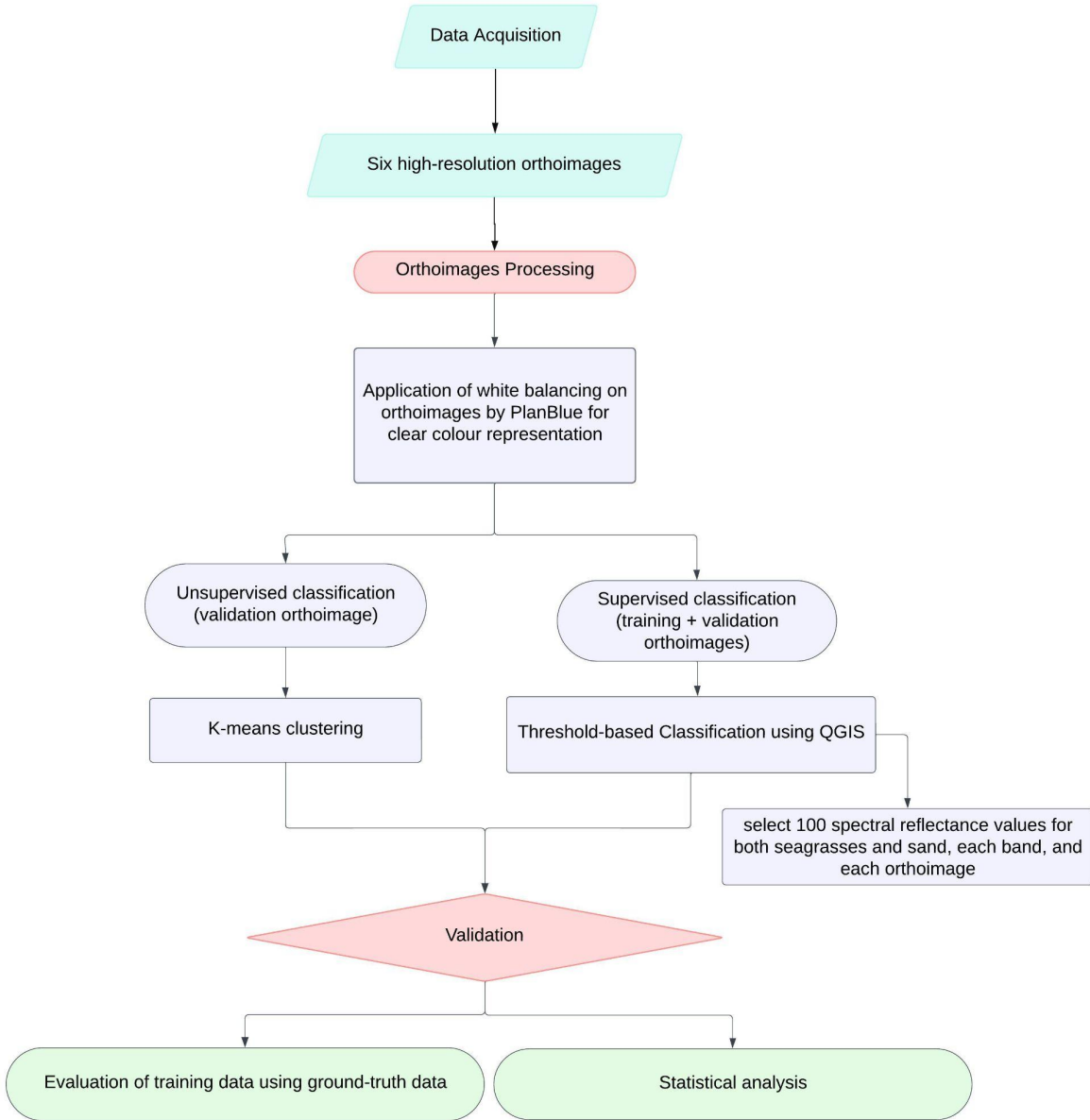
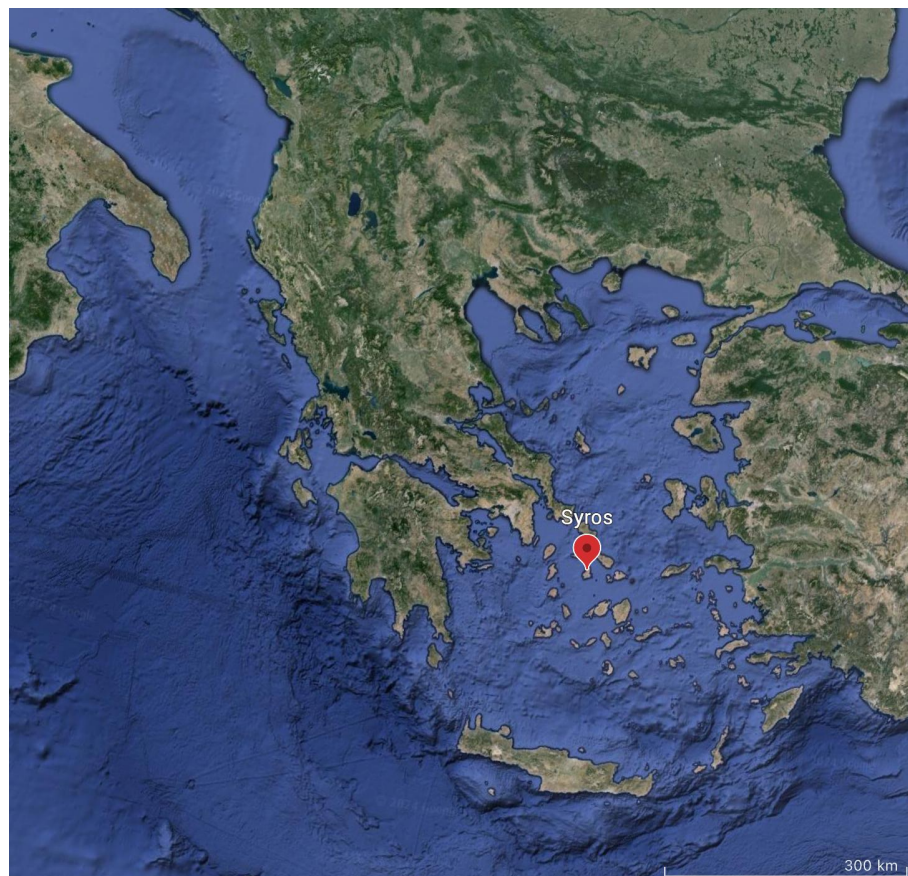


Fig. 10: Flowchart of the data acquisition and processing steps for orthoimages

4.6 Sentinel-2 imagery processing

First, there was an attempt to map seagrass ecosystems using S-2 imagery and the European Atlas of the Seas. This interactive tool made by EMODNet is helpful in showing seagrass ecosystems, and more specifically *P. oceanica*, across Europe. Code snippets from '[Cloud-Based RS with GEE: Fundamentals and Applications](#)' by Cardille et al. (2024) were used in this stage.

The preprocessing stage consisted of defining the bands - specifically B2 (blue), B3 (green), B4 (red) and B8 (Near-Infrared). All S-2 images from May to August 2023 (seagrasses' maximum productivity) are selected on GEE (Pirc 1986). The first region of interest (ROI) focuses on the island of Syros, Greece (Fig. 11). This location was chosen due to the presence of a high number of pixels on the EMODNet map, compared to other islands in the Eastern Mediterranean (Fig. 11). Images with less than 40% cloud cover were selected.



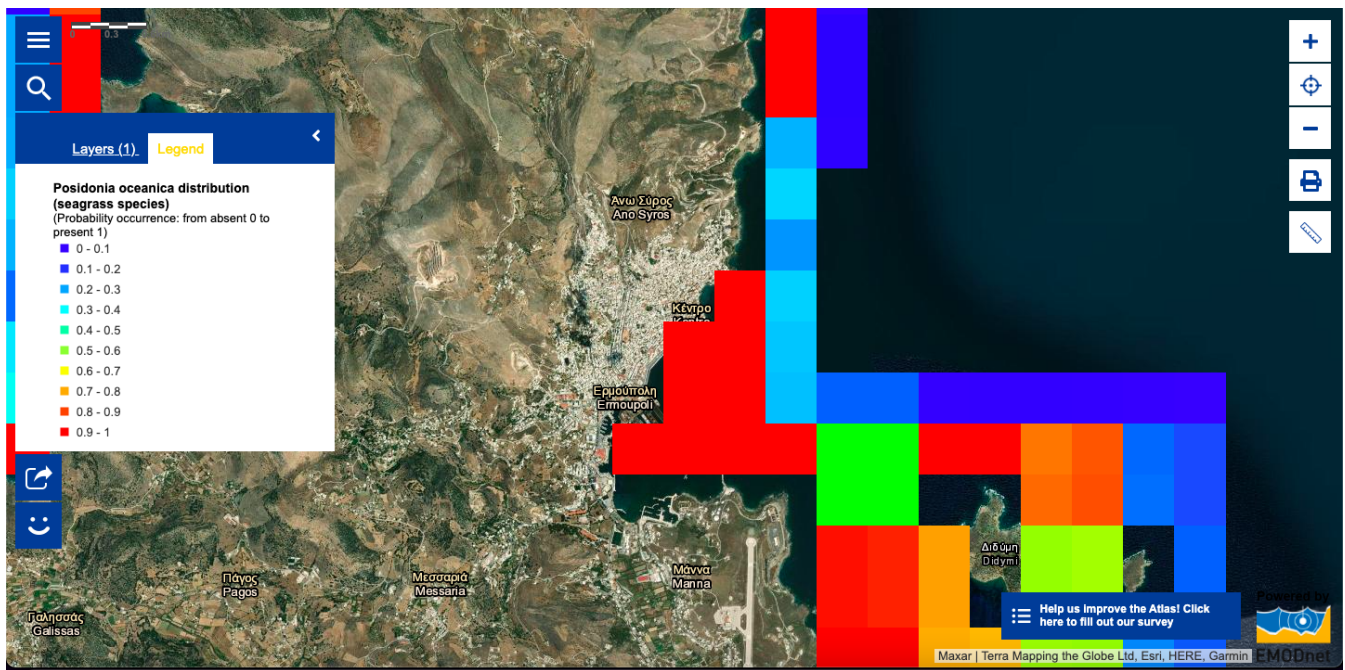


Fig. 11: Top: Syros Island on a map. Bottom: The European Atlas of the Seas by EMODNet showing *P. oceanica*' distribution around Syros Island. Legend shows seagrass distribution from absent 0 (blue) to present 1 (red).

4.7 Classification

Training and validation points for the classification were created within GEE, through a visual inspection of the EMODNet map (Fig. 12).

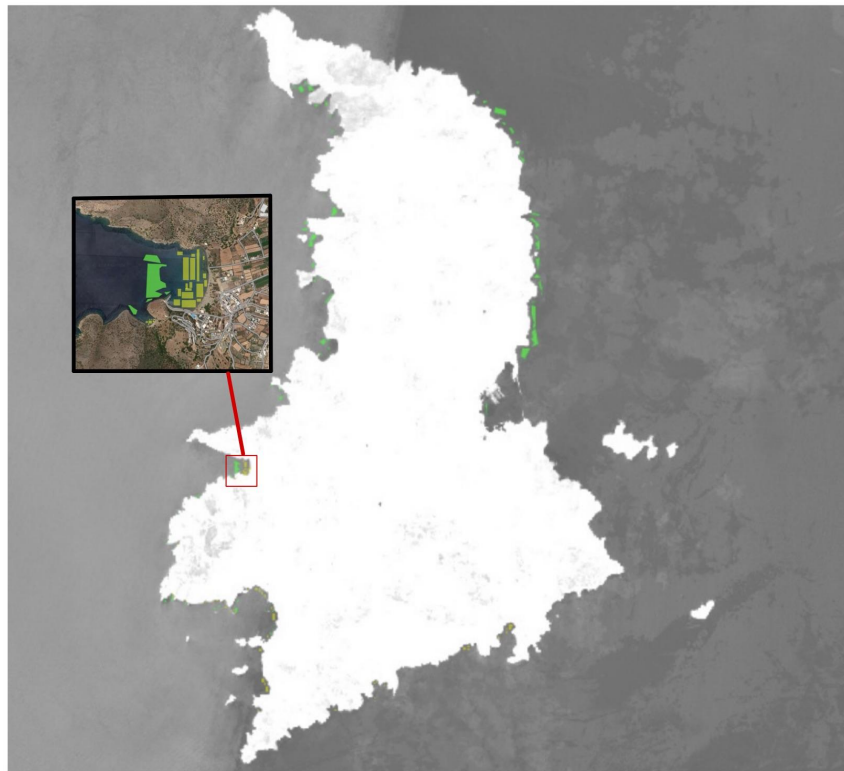


Fig. 12: Grayscale map of Syros Island, white representing land and grey water, green polygons can be spotted along the shores, representing seagrasses. Zoomed into the satellite imagery, with polygons differentiating seagrass (green) from non-seagrass (yellow) drawn through comparison with the European Atlas of the Seas' pixels.

The RF classifier was chosen to classify S-2 images. This added multiple decision trees to create predictions. The classifier was trained using the ‘sampleRegions’ method to associate spectral data with each sample. For validation, the classifier’s predictions on a separate set of data (‘validationData’) were compared with true classifications to compute an error matrix. However, due to unavailable Band 2 information, GEE encountered an error and consequently did not produce an accuracy assessment. The methods employed in this study are summarised in a comprehensive flowchart, as depicted in Figure 13.

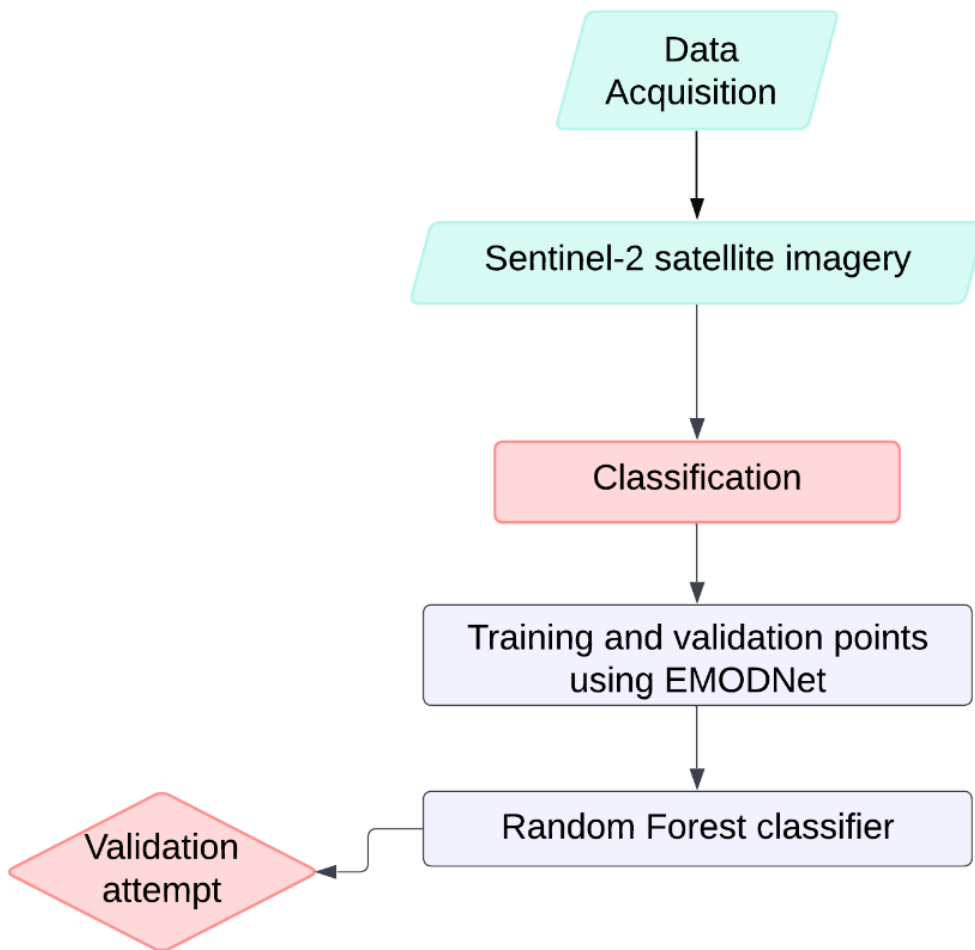


Fig. 13: Flow chart for Sentinel-2 methodology

4.8 Pixel size comparison

The resolutions from the S-2 image and the validation orthoimage were compared. The orthoimage's pixel size being approximately 0.2 cm, fine details were visualised on small areas. This estimation is crucial for acknowledging the spatial resolution of the orthoimage and its comparison with a multispectral imagery resolution (S-2), which has a lower resolution of 10 metres per pixel. The area covered by the validation orthoimage is 20.9 metres times 10 metres. The total pixels in this orthoimage are approximately 52,000,000, compared to 4 pixels in total in the S-2 image (see Fig. 19). Therefore, there are approximately 13,000,000 times more pixels in the orthoimage compared to S-2 in the same ROI. This shows that a single S-2 pixel covers the same area as 25,000,000 orthoimage pixels. The pixel size of the orthoimage is 5000 times higher than the S-2.

To align the orthoimage's resolution with that of S-2's 10-metre resolution, the image was processed on QGIS where it was aggregated to coarser resolutions. Initially a 10-metre per pixel resolution was set and later resolutions of 1, 0.5 and 0.05 metres per pixel were examined to observe the change in mapping accuracy.

5. Results

5.1 Orthoimages and Ground-truthing

A spectral signature comparison chart indicates distinctive reflectance patterns for each orthoimage's bands (Fig. 14). There is a consistent trend with each band showing similar reflectance values, and a decrease from orthoimage 1 to orthoimage 6 for seagrasses, spanning from 100 to 170 on an 8-bit scale (Fig. 14). Similarly, for sand, the same trend is followed, nevertheless the reflectance values start with 180 and go to 230 on an 8-bit scale (Fig. 14). The sixth orthoimage reflects the average spectral characteristics of the studied area, with its values derived from the mean of the average reflectance values across the training orthoimages (Fig. 14).

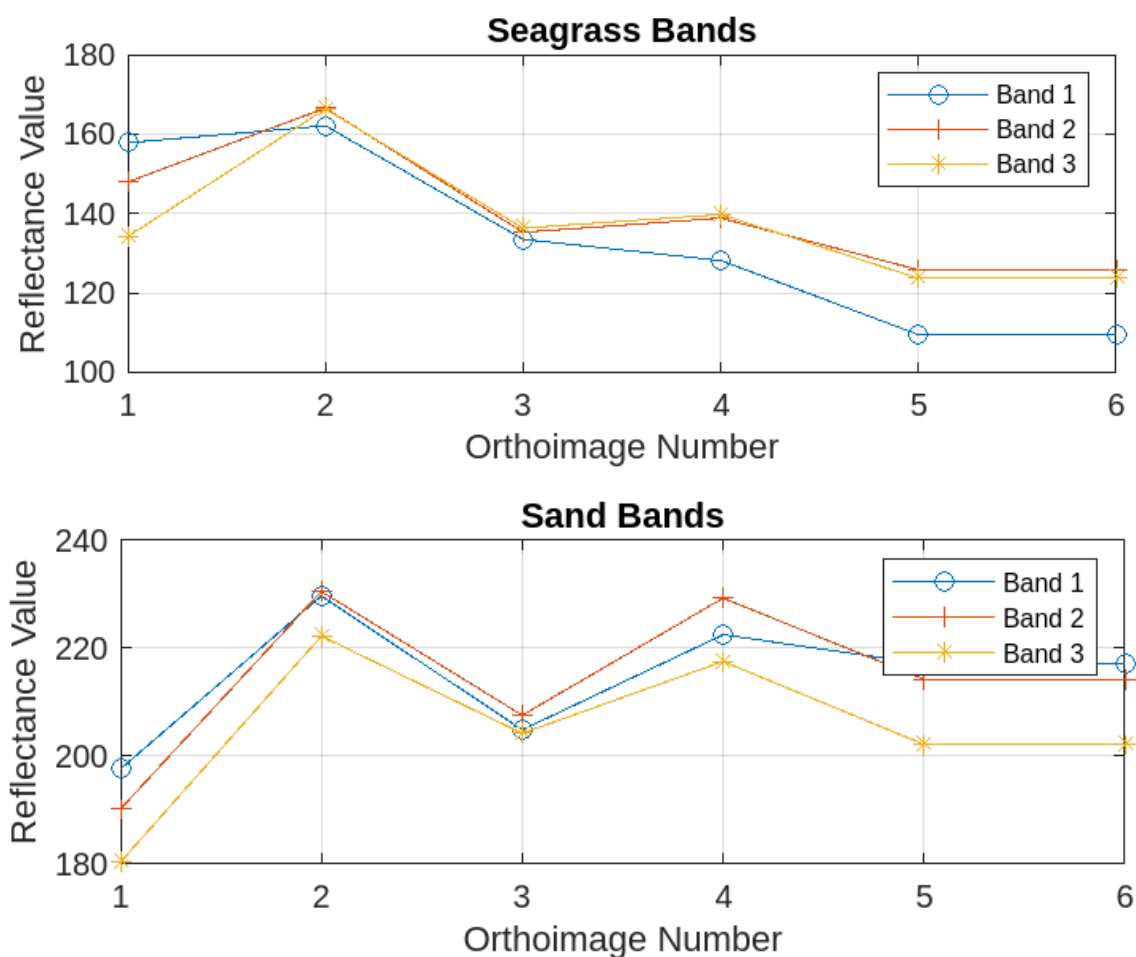


Fig 14: Band values identified using the ‘Select Feature’ tool on QGIS for the sand patch in Fig., for each orthoimage and on an 8-bit scale

Looking at spatial distributions, each orthoimage represents distinct patterns of seagrasses and sand (Fig. 15). The patterns are extremely varied, with some images displaying dense clustering of seagrass (orthoimages 2, 4 and 6) and others exhibiting more sparse and striped patterns (orthoimages 1, 2 and 4), most probably due to the direction of wave movement (Fig. 15). It is also clear that the camera capturing these orthoimages cast shadows along the edges, which can be misinterpreted as seagrass by geographic information systems such as GEE (Fig. 16). In orthoimage 5, seagrasses have a less defined pattern, similarly, the validation orthoimage shows a complex pattern, with seagrasses and sand distributed along the entirety of the region (Fig. 15).

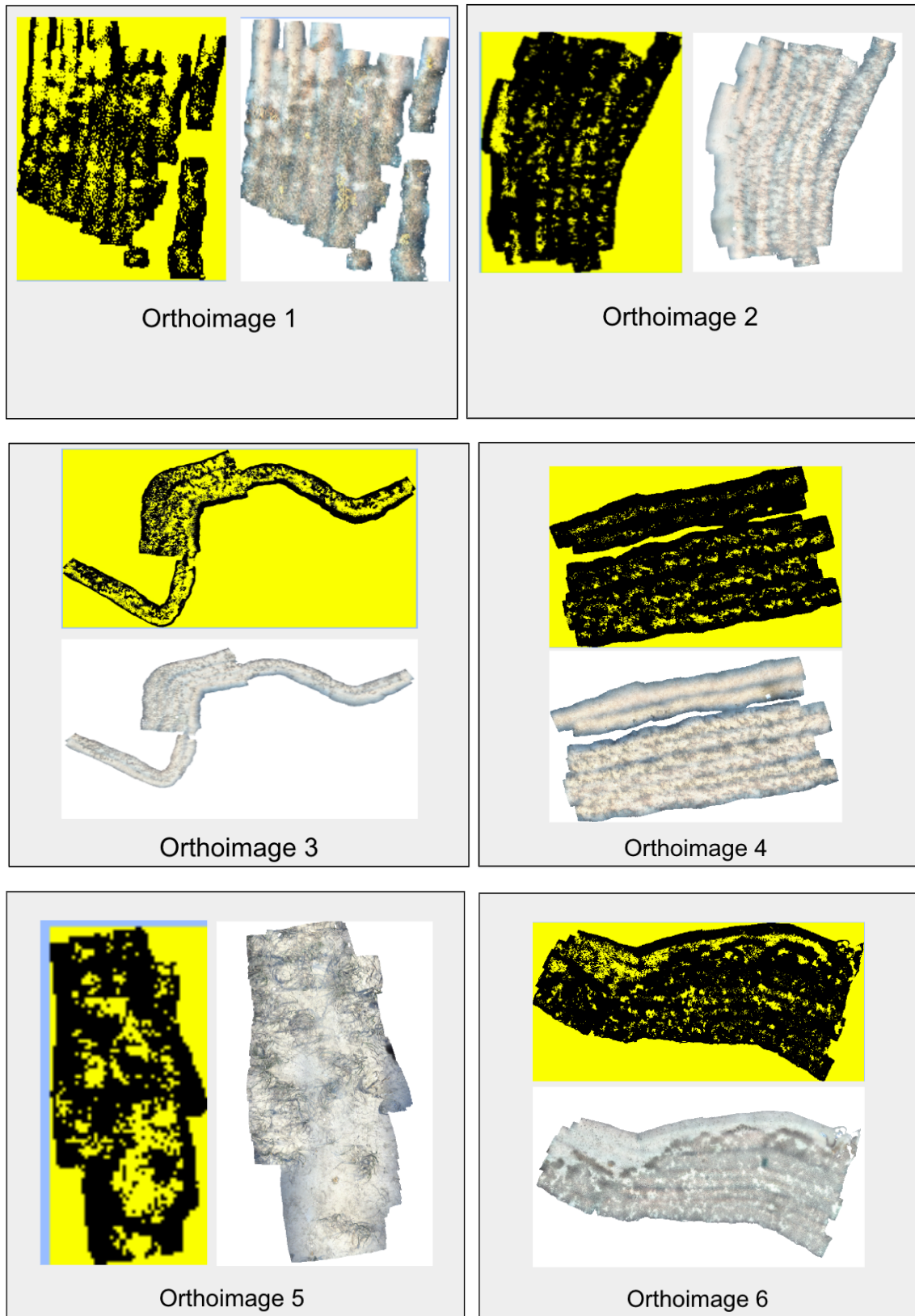
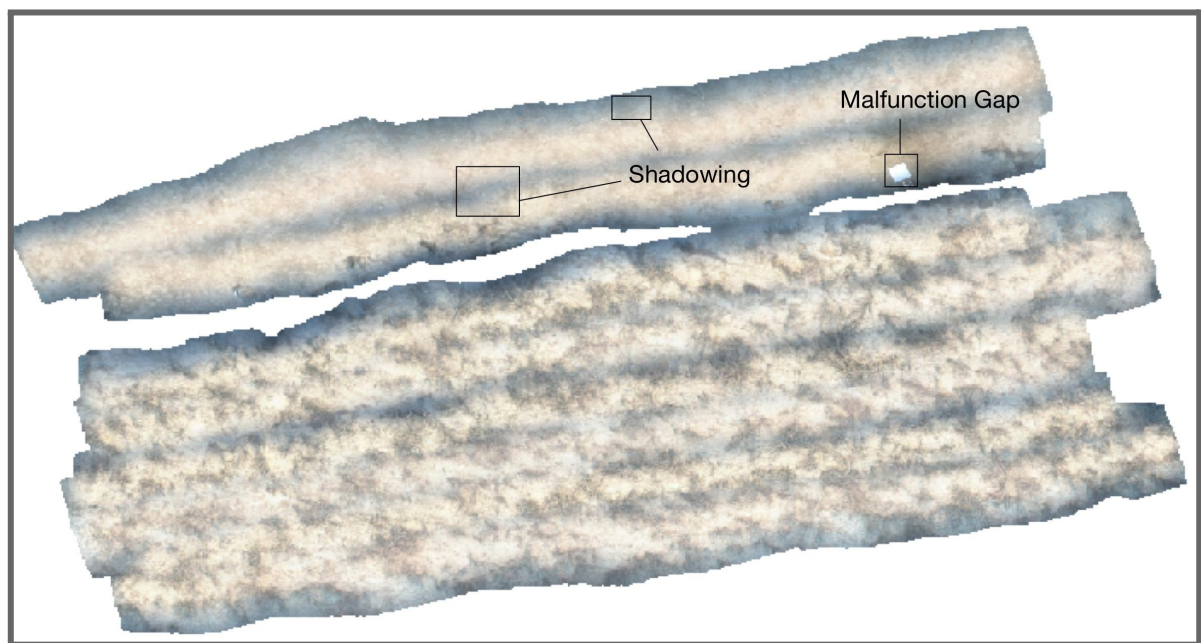
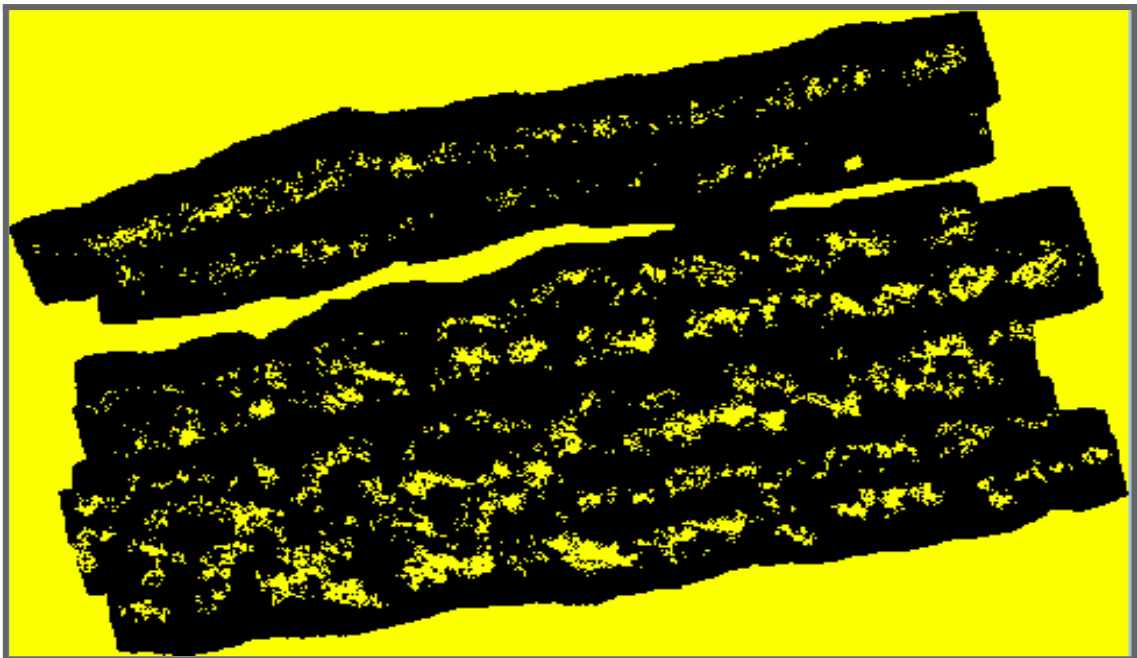


Fig. 15: Display of classified (left) and unclassified (right) orthoimages. Black: seagrass, Yellow: sand.



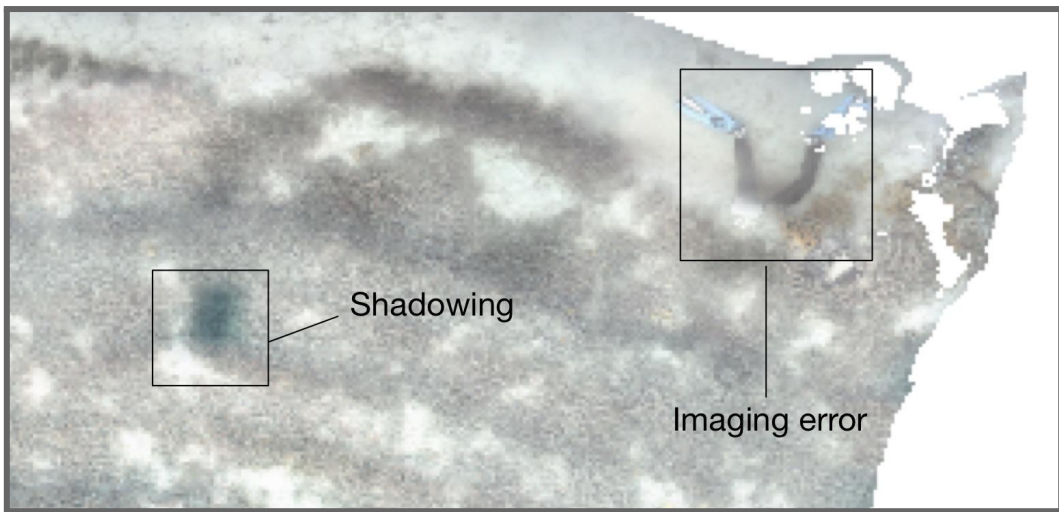


Fig. 16: Top: Classified orthoimage 4. Middle: Orthoimage 4 anomalies. 'Malfunction Gap' indicates a section where imaging was not captured due to potential camera malfunction. 'Shadowing' refers to areas where the camera casts shadows. Bottom: Orthoimage 6 anomalies. 'Imaging error' identifies the unintentional inclusion of a diver in the imagery.

The quantification of seagrass distribution within orthoimages requires an examination of each orthoimage's total area (Table 4). The seagrass extent, determined using GEE, coupled with calculations derived from metadata, reveal variations among orthoimages (Fig. 17). While orthoimage 4 does not have the largest area (132.20 m^2), it displays the largest seagrass extent among orthoimages (Table 4) (Fig. 17). Orthoimage 5 has the smallest area (4.67 m^2), however displays the second largest seagrass coverage (Table 4) (Fig. 17). This suggests that the seagrass density in the location of orthoimage 4 is high compared to that of the much larger areas captured in orthoimages 2 and 3 (158.56 m^2 and 523.13 m^2) (Table 4) (Fig. 17).

Table 4: Total area of each orthoimage (in m^2)

Orthoimage	Total area in m^2
1	30.5
2	158.56
3	523.13
4	132.20
5	4.67
6	209.10

Seagrass Coverage as a Percentage of Total Area for Each Orthoimage

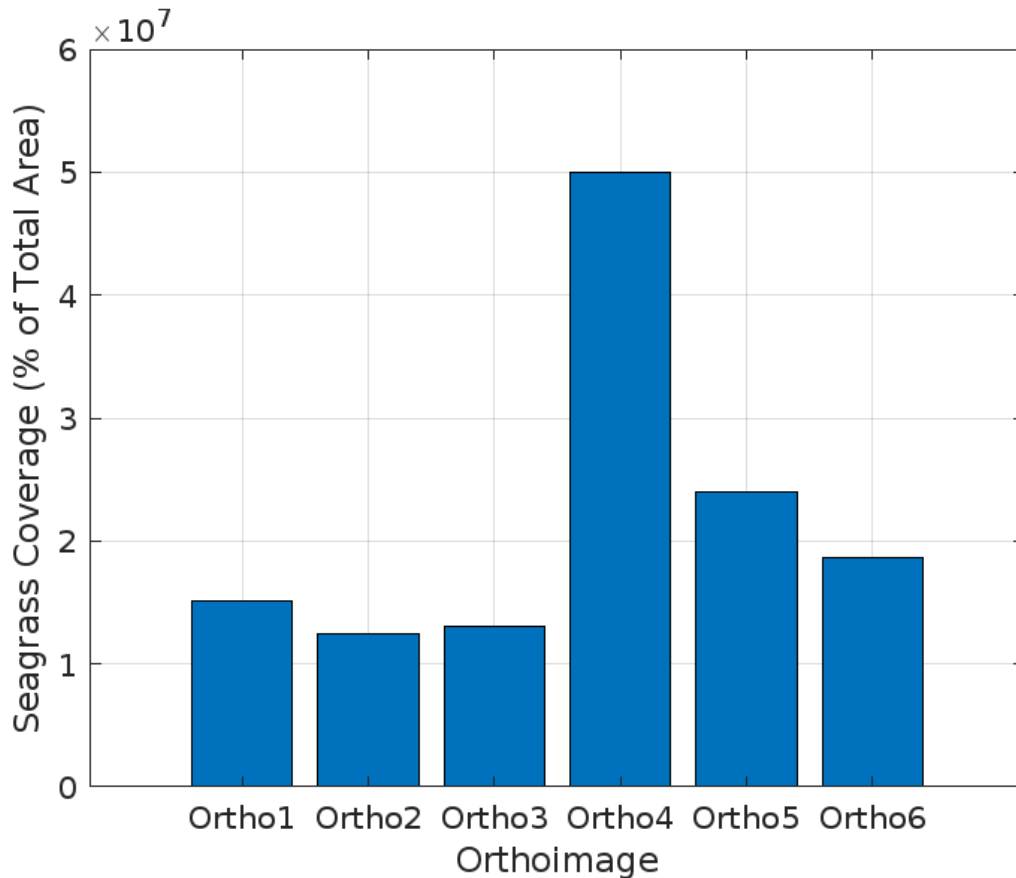


Fig. 17: Seagrass coverage shown as a percentage of the total area (in m^2) for each orthoimage

5. 2 Classification Results and Accuracy Assessment

There are 144,113 true positives (TP), meaning that 144,113 seagrasses were correctly classified and 18,936 instances of seagrasses were incorrectly classified (false negatives (FN)) (Table 5).

Table 5: The validation orthoimage's error matrix

	1	2
--	---	---

0	9,851	259
1	144,113	45,357
2	0	0
3	9,085	25,407

The accuracy for a single class was determined:

$$Accuracy = \frac{TP}{(TP + FN)}$$

$$Accuracy_{seagrass} = \frac{144,113}{144,113 + (9,851+9,085)}$$

$$Accuracy_{seagrass} = 0.8838631331685567$$

The calculated accuracy for seagrass classification, based on the error matrix, is approximately 88.39%. This indicates that about 88.39% of seagrass instances in the ground truth data were correctly identified by the classifier.

5. 3 The European Atlas of the Seas and Sentinel-2

The first attempt to use S-2 images and the European Atlas of the Seas resulted in a binary classification, displaying a colour palette of red for seagrass and green for non-seagrass (Fig. 18). Although ‘landMask’ has been applied, seagrasses are only present on land and green represents water, creating a simple map of land and water instead of showing selected features (Fig. 18).



Fig. 18: Map of Syros Island generated on GEE after the binary classification process. Red: seagrass, Green: non-seagrass.

5.4 S-2 classification results compared with orthoimages' classification

Using the ‘ee.Image.clip(geometry)’ function on GEE, an image can be clipped to a specific region (Fig. 19). There is only one S-2 image found on the validation orthoimage’s ROI, and it was taken between the 16th May and the 19th May 2023 (the orthoimage was acquired six days later, from the 25th May to the 28th May 2023). This image was clipped on the orthoimage to show the resolution contrast (Fig. 19). There is a clear distinction in pixelation shown by the overlay of S-2 (present in between four pixels) and the orthoimage beneath, highlighting the differences in spatial resolutions, with an extremely detailed orthoimage, where every feature seems to be visually defined, and the S-2 image with a coarser resolution, and potentially lost information on features (Fig. 19).

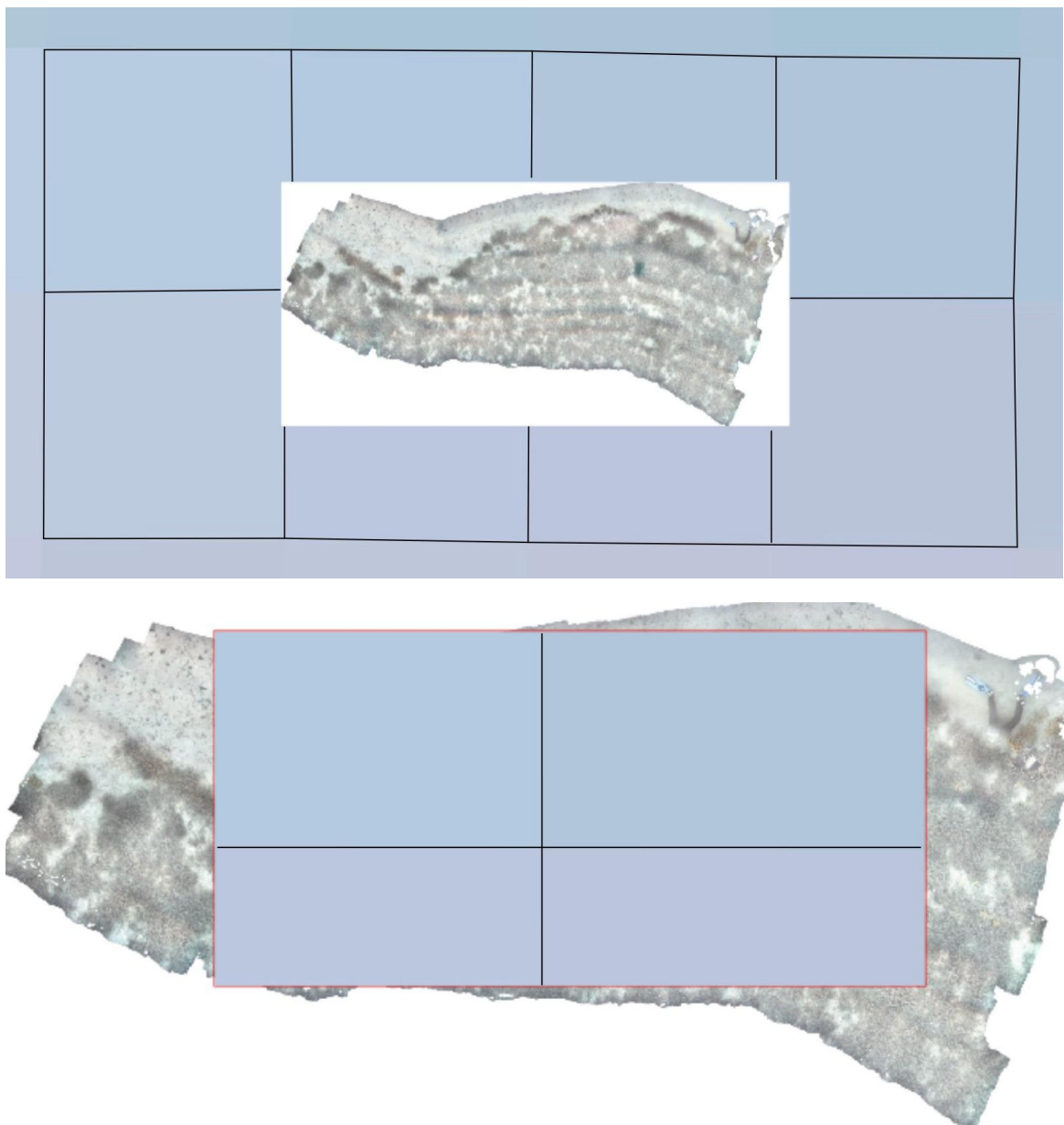


Fig. 19: Top: Overlay of the validation orthoimage on S-2 imagery, pixels outlined. Bottom: Overlay of S-2 imagery on the validation orthoimage, pixels outlined.

The orthoimage histograms display a broader distribution of pixel values, indicating substantial variability within the data (Fig. 20). Conversely, the S-2 histograms exhibit a narrower range of pixel values (Fig. 20). The orthoimages' frequency distributions span pixel values from approximately 180 to 240, showcasing a diverse range in the dataset, while the S-2 reveal data concentrated at specific values: around 2600 for Band 2, 2300 for Band 3 and 2100 for Band 4 (Fig. 20). The frequency pattern for S-2 data is extremely limited, going from the counts of one to three, indicating a lower frequency range compared to the six-hundred times higher frequency observed in the orthoimage data (Fig. 20).

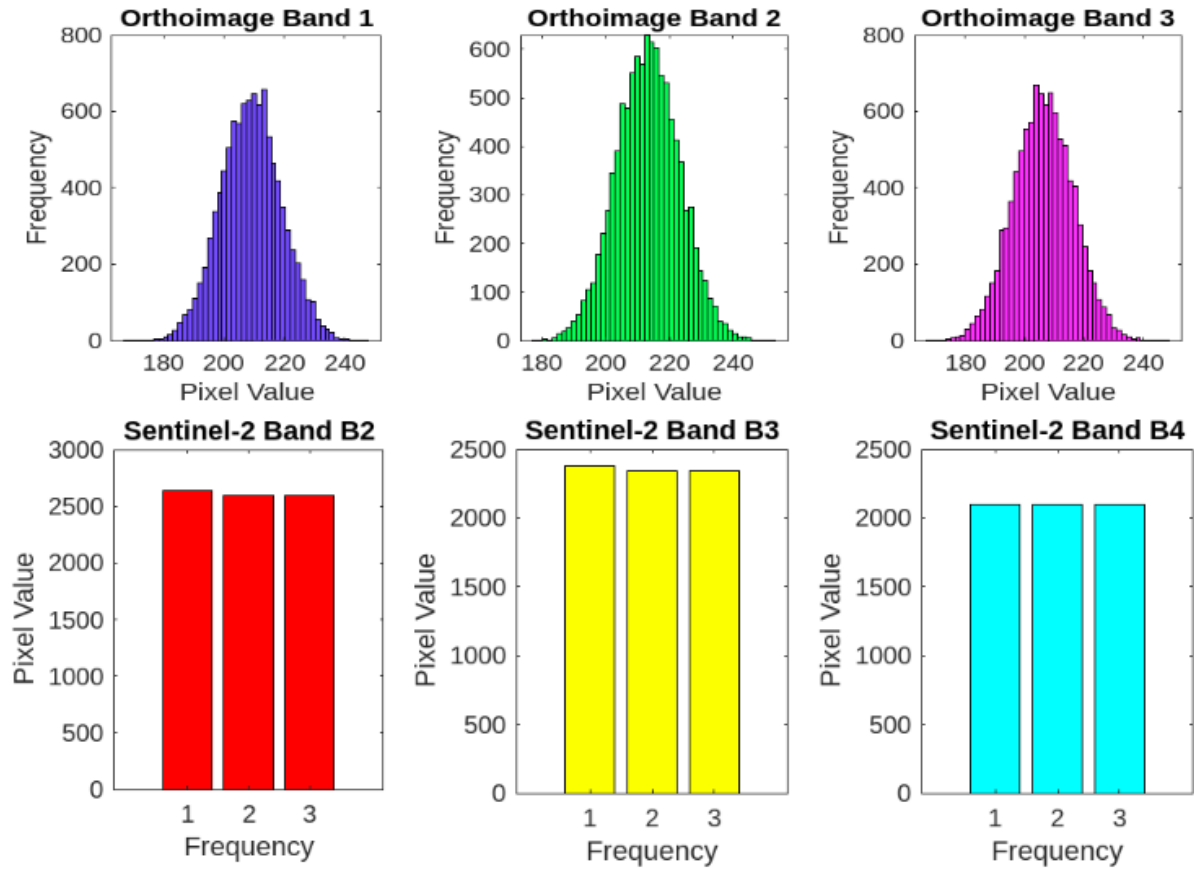


Fig. 20: Frequency distributions of pixel values for every band of the orthoimage and S-2

5.5 Accuracy Assessment at reduced resolution for the orthoimage

Following Traganos et al. (2018), the study area was divided into sub areas for focused analysis and bands down-scaled for compatibility with S-2's resolution (Fig. 21). First, the orthoimage was aggregated to 10 m/pixel to match the S-2 resolution and understand the accuracy (Fig. 21). The classification process was assessed using an error matrix and an overall accuracy at 10 m/pixel resolution, displaying 46% accuracy. Visually, the seagrass coverage covers the entire ROI (Fig. 21). At 1 m/pixel, the predicted seagrass coverage is 50%. At 0.5 and 0.05 m/pixel, the classification becomes more visible (Fig. 21).

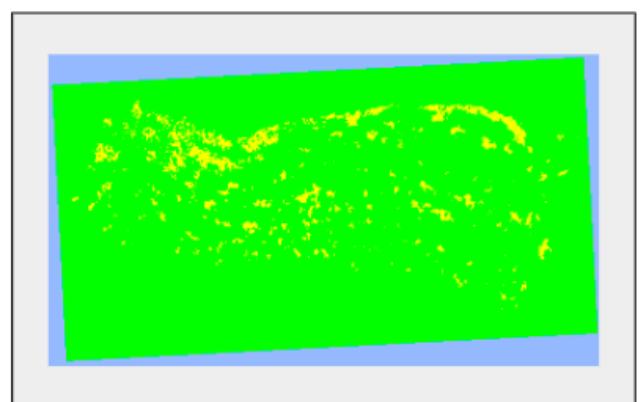
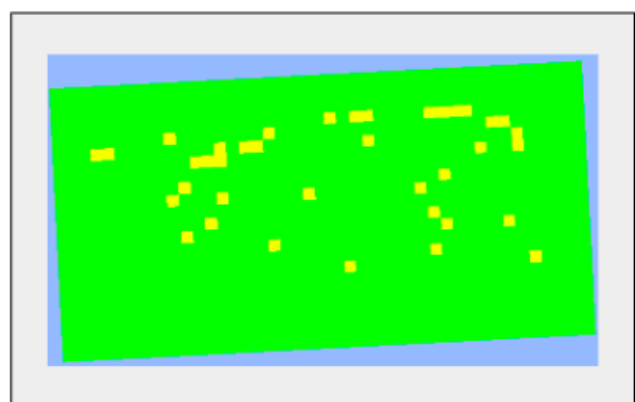
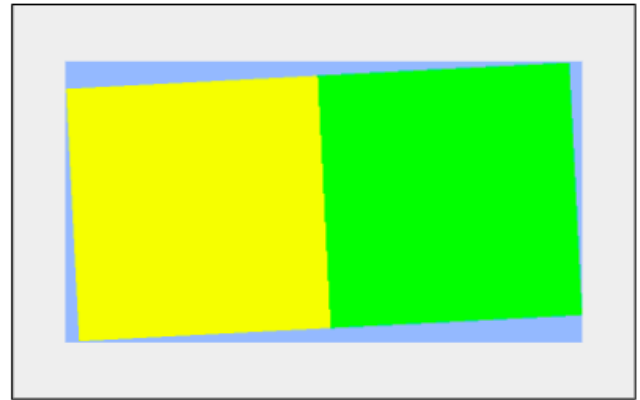
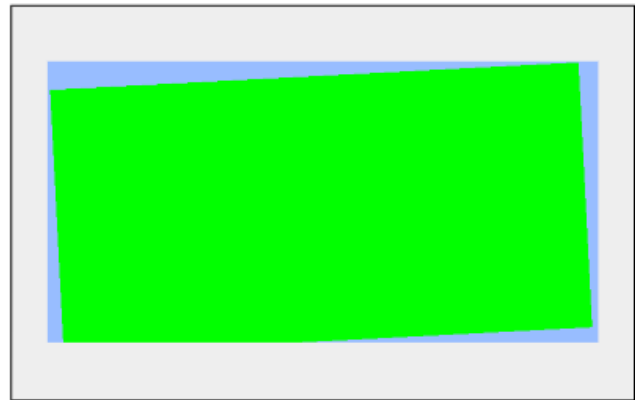


Fig. 21: Downscaling validation orthoimage's resolution at 10 metre-per pixel (a), at 1 metre-per pixel (b), at 0.5 metre-per pixel (c), at 0.05 metre-per pixel (d).

6. Discussion

6.1 Orthoimage Classification and Accuracy

The use of high-resolution orthoimages is crucial for achieving the necessary accuracy to validate a model. Detail-rich imagery can efficiently map seagrasses and distinguish different underwater features (Fig. 22). The preprocessing steps enhance the reliability of the classification by amplifying the spectral signatures of seagrasses, making them even more distinguishable (Fig. 22).



Fig. 22: A close-up view of a seagrass patch taken from the validation orthoimage until pixels are clear.

GEE proves to be an ideal platform to process large datasets, supporting a targeted analysis up to a certain extent. Although the threshold-based method simplifies the classification process and shows little variation across the orthoimages, this relies on predefined threshold values which may not apply in the most coherent way to different geographic locations due to spectral differences in seagrass beds (Fig. 7) (Table 3). The binary classification distinguishes between seagrass and sand classes, focusing solely on whether seagrass is present or absent, thereby enhancing the clarity of the results and establishing a decision threshold. Following the training data's classification process, the validation phase plays a fundamental role in assessing the effectiveness of the classification model. The approach of combining both unsupervised and supervised classifications combines the strengths of both methods (Fig. 9). As mentioned, the classification's reliability is also ensured by the ground truth data (Fig. 8). An error matrix is made to provide a quantitative assessment of the model's accuracy, which, in the case of seagrass identification, is high, at 88.39%.

Looking at seagrass distribution relative to orthoimage size, a smaller orthoimage can have a higher seagrass density than larger ones (Table 4) (Fig. 17). For instance, orthoimage 5, despite its smallest size, demonstrates a higher seagrass coverage compared to some of the larger orthoimages (Table 4) (Fig. 17). This observation emphasises that the seagrass coverage proportion is not only determined by the size of the orthoimage but also by the specific characteristics of the location from which the image was taken. Anthropogenic activities affect seagrass distributions, yet other influences also exist (Avcı 2005). Among these, the Kemerköy thermal power plant located in the Northern coast of Gökova changes physical and chemical parameters of the water, thereby affecting seagrass growth (Avcı 2005). The geological history of the seafloor may play a role in shaping the current seagrass distribution pattern (Şener & Tüfekçi 2008). Orthoimage 2, displaying the least extent of seagrass coverage and located approximately 5 km North from orthoimage 4 -- which shows the most extensive seagrass coverage --lies on Middle Miocene formations, unlike the Lower Miocene substrates for all other orthoimages (Fig. 6) (Fig. 17) (Şener & Tüfekçi 2008). Northern Gökova has a karst topography, which can lead to the emergence of freshwater springs and change the water chemistry, including salinity levels of nearby marine environments (Barlas et al., 2012). The geomorphological features can be a potential influence on seagrass distribution, yet there is a critical gap in current research on the topic.

Understanding the influences on seagrass coverage could provide insights crucial for ecological assessments.

Acknowledging the extent of seagrass coverage in relation to each orthoimage's total area, considering both environmental and human impacts, is fundamental for in-depth ecological assessments.

6. 2 High-resolution data limitations

When classifying orthoimages, it is essential to consider certain constraints, particularly those associated with the acquisition of underwater imagery. An important limitation is the presence of uniform dark areas along the edges of each orthoimage, originating from the shadowing effects of the underwater camera (Fig. 16). These shadowed areas are frequently misclassified as seagrass -- a prevalent challenge in RS -- and they can compromise the accuracy of the classification (Fig. 16). Distinguishing between seagrasses and shadows is complicated due to this issue. Nevertheless, seagrasses can still be identified through their organic shapes and continuity, in contrast with linear and consistent patterns cast by shadows (Fig. 15). Consequently, orthoimages represent complex and dynamic seagrass beds, capturing their distributions across images, yet influenced by the imaging process itself.

Another challenge worth noting is that quality orthoimages require extensive fieldwork, involving trained divers to operate underwater cameras equipped with specialised sensors (Fig. 23). Divers need to consider seagrass ecosystems' varying depths, requiring expertise in navigation and equipment capable of functioning under different pressure conditions.



Fig. 23: Example of hyperspectral camera called DiveRay used by PlanBlue at Finger Reef (Mills et al., 2023).

The images must be processed to enhance visibility and contrast. Handling these multispectral datasets is computationally intensive, requiring advanced software and technical expertise for efficient processing and preparation for classification.

Once these requirements are acknowledged, including the imaging limitations, the cost can be evaluated. Conducting fieldwork, acquiring specialised equipment and trained divers are resource-intensive and costly. Evaluating the trade-off between the benefits of high-resolution imagery and its associated cost is essential.

6. 3 Software limitations and threshold-based approach

Although the main limitation in this research stands as the resolution of S-2 imagery, it is also critical to note that GEE imposes important restrictions. For instance, it does not support powerful classifiers like RF to be applied on orthoimages due to internal errors, such as Internal Error Code 13, which typically occurs when the dataset used is too large. This machine learning approach is recognised for its superior efficiency and accuracy compared to simpler threshold-based methods.

6. 4 Comparative Analysis with S-2 data

The S-2 analysis, focusing on the island of Syros, shows the constraints of using binary classification in capturing details on seagrass beds (Fig. 12). The training dataset sourced from EMODNet's *P. Oceanica* distribution map is inadequate for such an analysis (Fig. 11). Despite selecting the time of year based on the ecosystem's maximum productivity, masking clouds, and using the widely recommended RF classifier, the primary issue lies with the training data's inability to accurately represent seagrasses, leading to a simplistic land and sea portrayal (Fig. 18). The satellite imagery's limited resolution further compromises classification accuracy.

6 . 5 Resolution's impact on mapping seagrasses

The marked disparity in resolution between orthoimages and S-2 imagery necessitates the identification of an appropriate S-2 resolution to match the accuracy obtained from orthoimages.

Yet, attempting to decrease the spatial resolution differences presents significant challenges. To match the orthoimages' resolution with that of S-2, approximately 25,000,000 orthoimage pixels would need to be aggregated into a single Sentinel-2 pixel. However, GEE's processing constraints limit the number of input pixels that can be compressed into a single output pixel to 65,536, far below the 25,000,000 pixels required for matching the S-2 resolution — a factor about four hundred times greater than GEE's processing capabilities.

Reducing the orthoimage resolution to 10 metre-per pixel to match S-2 still resulted in a resolution about five hundred times finer than S-2's (Fig. 21). This downscaling effort achieved a 46% accuracy rate, which is inadequate since the seagrasses span the entirety of the orthoimage. Similarly, at 1 metre-per pixel, the classification shows seagrasses covering half of the ROI, which fails to meet acceptable classification standards (Fig. 21). At 0.5 and 0.05 metres per pixel, the classification accuracy improves to 53%, however, accurately distinguishing between the two classes remains challenging (Fig. 21). These resolutions are

still much finer than S-2's, demonstrating the freely-accessible satellite imagery's inefficiency.

From a broader context, this research highlights the significant influence of resolution on the accuracy of seagrass mapping. While a high resolution (88.39%) allows the classifier to differentiate between classes and capture detailed features accurately, a coarser resolution (1 m/pixel) decreases the accuracy to 50%, weakening the distinction between seagrass and non-seagrass (Fig. 21).

The insufficient resolution quality of S-2, in addition to GEE's computational limitations, emphasises the necessity for innovative approaches to monitor seagrass habitats. The introduction of PlanBlue's advanced underwater drone technology for ecosystem mapping offers a promising path towards improving seagrass mapping, playing a significant role in marine conservation and efforts to mitigate climate change.

6. 6 Broader implications of findings

From a broader perspective, this study emphasises the critical importance of adopting advanced RS techniques for effective conservation and monitoring strategies. Through detailed mapping, this study shows areas with high seagrass biodiversity and carbon storage potential, and can assist in prioritising conservation efforts in regions most critical for biodiversity and climate regulation. Moreover, this research hopes to pave the way for further studies to assess changes over time, thereby contributing to ongoing efforts to monitor and understand how these ecosystems evolve. Furthermore, this study aims to set a foundation for further research to examine evolution over time, thereby supporting current efforts to monitor and comprehend the dynamics of these habitats.

The freely accessible satellite data can be invaluable in broad-scale monitoring as an initial assessment, however is proven to be inefficient in capturing fine-scale details necessary for mapping these complex ecosystems. This study therefore highlights the gap between the available technology and conservation science's needs.

Conclusion

In the context of climate change, seagrass ecosystems' preservation has never been more imperative. Seagrass systems are fundamental actors in sequestering carbon, offsetting emissions through natural processes. This study focuses on *P. oceanica*, the most ecologically significant species in the Aegean Sea through its ecological services, but also its role as a carbon sink (Duman et al., 2019). This places the species in the centre of the BC strategy in mitigating climate change. The understanding of these ecosystems is crucial from an environmental science, policy, and technology perspective.

RS techniques have become a transformative step in ecosystem monitoring, giving the ability to map habitat distributions. This study looks at high-resolution orthoimages and S-2 satellite data in mapping these habitats with great accuracy. The comparative analysis showed the constraints of depending on freely available satellite imagery, proving it to be unreliable, therefore determining high resolution imagery's necessity. Obtaining advanced imaging represents an important tool in conservation, providing the visualisation and quantification of the habitats with clarity and accuracy.

Nevertheless, this innovative way of monitoring may not always be the preferred approach. Acquiring high-resolution imagery is a demanding task. Despite offering exceptional results, this method faces equipment-related, logistical, and computational needs. Careful planning and collaborative efforts are essential to address these issues, requiring the combination of expertise from scientists and stakeholders.

To overcome these challenges, the research calls for the development of a cost-efficient software, with adaptable cloud-based workflows, and capable of using machine learning algorithms to support extensive datasets like high-resolution orthoimagery. It is through these technological advances that conservation efforts can be assisted and become effective for marine ecosystems to be preserved.

The urgency for conservation was juxtaposed with the economic and ecological value of seagrasses, reinforcing the need for sustainable management practices to protect these habitats for future generations. Acknowledging seagrass meadows as crucial BC ecosystems

not only emphasises their importance in supporting biodiversity, but also shows their potential to mitigate climate change through carbon sequestration. This dual benefit highlights a compelling incentive for businesses to invest in the conservation of these habitats, offering a pathway to achieve their sustainability goals while participating in the global effort to combat climate change through effective carbon offsetting strategies.

There are multiple initiatives which must be considered to preserve these ecosystems. This should include the control and treatment of sewage to reduce nutrient, organic matter and chemical loading in the sea, the regulation of land reclamation and use, sustainable aquaculture and fisheries, and raising awareness on the importance of these habitats. These are initiatives which can be achieved through MPAs, just like the MCS does.

This study presents a call to action to preserve vital marine ecosystems, through an interdisciplinary collaboration among remote sensing experts, software engineers, marine scientists, businesses, and policy-makers to overcome the logistical and computational challenges in obtaining and processing high-resolution imagery.

Auto-critique

Reflecting on this research, I am confident it has successfully met its aims and objectives, particularly in the area of seagrass mapping within the chosen study sites. The achievement of an 89% accuracy rate in mapping these ecosystems highlights the efficiency of the methodologies and the potential remote sensing technologies have for environmental efforts.

A significant part of this study was the exploration of Sentinel-2's limitations, a crucial section for guiding future research in the field. The process of coding in Java on Google Earth Engine presented a great challenge, given my lack of prior experience with this programming language and this software. Nonetheless, overcoming the complexities associated with Java and GEE has been a fulfilling experience, representing a considerable achievement in my technical abilities.

Another important challenge I encountered was the lack of training and ground-truth data for Sentinel-2. This was particularly due to a lack of precise data and efficient software needed to map Gökova Bay. Moreover, the orthoimages were immensely large datasets, which made their upload onto multiple software platforms very time-consuming.

The limitations of GEE further exacerbate these challenges, specifically due to its inability to support the application of machine learning algorithms on high-resolution orthoimages. This constraint necessitated manual selection of threshold values for each seagrass and sand patches across each orthoimage, a process which was extremely time-intensive.

Another significant obstacle in the research was the attempt to explain the underlying causes of differences in seagrass coverages between study sites very close to each other, a task made difficult by the lack of research in this area.

Despite these challenges, I am confident that this study provides a comprehensive overview of seagrass mapping techniques, putting forward the importance of conservation efforts (both past and ongoing), and calls for the critical need for such initiatives going

forward. By navigating through the multifaceted challenges presented during this research, the study does not only contribute to our understanding of seagrasses, but also sets a foundation for future research in marine environmental conservation.

References

- Akçalı, B. and Cirik, Ş. (2015) 'Marine Phanerogams (Seagrasses) of Turkish Aegean Sea', in Katağan, T., Tokaç, A., Beşiktepe, Ş., and Öztürk, B. (eds.) *The Aegean Sea Marine Biodiversity, Fisheries, Conservation and Governance*. Istanbul: Istanbul University, pp. [125-145].
- Appolloni, L., Buonocore, E., Russo, G.F., & Franzese, P.P. (2020). The use of remote sensing for monitoring *Posidonia oceanica* and Marine Protected Areas: A systematic review. Parthenope University of Naples and CoNISMa.
- Avcı, S. (2005) 'Türkiye Termik Santraller ve Çevresel Etkileri' [Thermal Power Plants in Turkey and Their Environmental Effects], *Coğrafya Dergisi*, İstanbul Üniversitesi Edebiyat Fakültesi Coğrafya Bölümü, no. 13, pp. 1-26. (In Turkish).
- Bakırman, T., & Gümüşay, M.U. (2020). Assessment of Machine Learning Methods for Seagrass Classification in the Mediterranean. *Baltic Journal of Modern Computing*, 8(2), 315-326. <https://doi.org/10.22364/bjmc.2020.8.2.07>.
- Barlas, M., İkiel, C. and Özdemir, N. (2012) 'Gökova Körfezi'ndeki akarsu kaynaklarının fiziksel ve kimyasal açıdan incelenmesi' [Physical and chemical analysis of river sources in the Gulf of Gökova], 65. Geological Congress of Turkey. (In Turkish).
- Bilecenoglu, M., & Çınar, M. E. (2021). Alien Species Threat across Marine Protected Areas of Turkey—An Updated Inventory. *Journal of Marine Science and Engineering*, 9(10), 1077. <https://doi.org/10.3390/jmse9101077>.
- Blasi, F. (2009) 'Il valore economico delle praterie di *Posidonia oceanica*' [The economic value of *Posidonia Oceanica*], *Biologia Marina Mediterranea*, 16, pp. 130-131. (In Italian).

Boudouresque, C.F., Mayot, N. and PerGeNt, G. (2006) 'The outstanding traits of the functioning of the *Posidonia oceanica* seagrass ecosystem', Biol. Mar. Medit., 13(4), pp. 109-113.

Brasier, M.D. (1975) 'An Outline History of Seagrass Communities', Palaeontology, 18(4), pp. 681-702.

Cardille, J.A., Crowley, M.A., Saah, D. and Clinton, N.E. (eds.) (2024) Cloud-Based Remote Sensing with Google Earth Engine: Fundamentals and Applications.

Duarte, C.M., Middelburg, J.J. & Caraco, N. (2005) 'Major role of marine vegetation on the oceanic carbon cycle', BG, 2(1), pp. 1–8. Available at:
<https://doi.org/10.5194/bg-2-1-2005>. Published 01 February 2005.

Duman, M. et al. (2019). Mapping *Posidonia Oceanica* (Linnaeus) Meadows in the Eastern Aegean Sea Coastal Areas of Turkey: Evaluation of Habitat Maps Produced Using the Acoustic Ground-Discrimination Systems. International Journal of Environment and Geoinformatics (IJEGEO), 6(1), 67-75. DOI: 10.30897/ijegeo.544695.

European Atlas of the Seas:

https://ec.europa.eu/maritimeaffairs/atlas/maritime_atlas/#lang=EN;p=w;bkgd=1;theme=631:1.00;c=2751000.0720948074.4498622.141796994;z=11.

Fornes, A., Basterretxea, G., Orfila, A., Jordi, A., Álvarez, A. and Tintoré, J., 2006. Mapping *Posidonia oceanica* from IKONOS. ISPRS Journal of Photogrammetry and Remote Sensing, 60(5), pp.315-322.

FOSS4G (2021) Improving Seagrass Detection Through A Novel Method For Optically Deep Water Masking [Video]. YouTube. Available at:
https://youtu.be/lR_dwpLSEM?si=UqPz2HhkXJ7UPy8s (Accessed: [8 November 2023]).

- Gomes, M., Silva, J., Gonçalves, D., Zamboni, P., Perez, J., Batista, E., Ramos, A., Osco, L., Matsubara, E., Li, J., Marcato Junior, J., & Gonçalves, W. (2020). Mapping Utility Poles in Aerial Orthoimages Using ATSS Deep Learning Method. Sensors, 20(21), 6070. <https://doi.org/10.3390/s20216070>.
- Gorelick, N., Hancher, M., Dixon, M., Ilyushchenko, S., Thau, D. and Moore, R. (2017) 'Google Earth Engine: Planetary-scale geospatial analysis for everyone', Remote Sensing of Environment, 202, pp. 18-27. doi:10.1016/j.rse.2017.06.031.
- Greenfield, P. (2023) 'Revealed: more than 90% of rainforest carbon offsets by biggest certifier are worthless, analysis shows', The Guardian. Available at: <https://www.theguardian.com/environment/2023/jan/18/revealed-forest-carbon-offsets-biggest-provider-worthless-verra-aoe> (Accessed 13 March 2024).
- Hein, L., Van Koppen, K., de Groot, R.S. & van Ierland, E.C. (2006) 'Spatial scales, stakeholders and the valuation of ecosystem services', Ecological Economics, 57, pp. 209-228.
- Kurt, O. and Öztürk, S. (2022) 'Observation of Marine Areas (Çandarlı and Gökova Bays) and Their Biodiversity', Sakarya University Journal of Science, 26(1), pp. 213-223.
- Koçak, M., Kubilay, N., Herut, B. & Nimmo, M. (2007) 'Trace Metal Solid State Speciation in Aerosols of the Northern Levantine Basin, East Mediterranean', Journal Name, 56, pp. 239–257. Published 19 December 2006.
- Lavery, P.S., Mateo, M.-Á., Serrano, O., & Rozaimi, M. (2013). Variability in the Carbon Storage of Seagrass Habitats and Its Implications for Global Estimates of Blue Carbon Ecosystem Service. <https://doi.org/10.1371/journal.pone.0073748>.
- Marbà, N., & Duarte, C. M. (2010). Mediterranean warming triggers seagrass (*Posidonia oceanica*) shoot mortality. Global Change Biology, 16(8), 2366-2375. This research

highlights the impact of water temperature on the mortality rates of *Posidonia oceanica* shoots, reflecting the sensitivity of the species to temperature variations.

McKenzie, L.J. & Yoshida, R.L. (2020) 'Over a decade monitoring Fiji's seagrass condition demonstrates resilience to anthropogenic pressures and extreme climate events', Marine Pollution Bulletin, 160, 111636. Available at: <https://doi.org/10.1016/j.marpolbul.2020.111636>. Published November 2020.

Mediterranean Conservation Society. (2023) 'Grantee', Conservation Media Group. Available at: <https://www.conservationmediagroup.org/grantee/mediterranean-conservation-society> (Accessed: [16 March 2024]).

MedPosidonia Network. (2023) 'Ecology', MedPosidonia Network. Available at: <https://medposidonianetwork.com/ecology/> (Accessed: [16 March 2024]).

Mills, M. S., UngermaNN, M., Rigot, G., den Haan, J., Leon, J. X., & Schils, T. (2023). Assessment of the utility of underwater hyperspectral imaging for surveying and monitoring coral reef ecosystems. *Scientific Reports*, 13:21103. <https://doi.org/10.1038/s41598-023-48263-6>.

Monnier, B., Pergent, G., Mateo, M.-Á., Clabaut, P. (2022). Quantification of blue carbon stocks associated with *Posidonia oceanica* seagrass meadows in Corsica (NW Mediterranean). Science of the Total Environment, 838.

Moniruzzaman, M., Islam, S.M.S., Lavery, P., Bennamoun, M. and Lam, C.P. (2019) 'Imaging and Classification Techniques for Seagrass Mapping and Monitoring: A Comprehensive Survey', [Preprint]. Available at: <https://arxiv.org/abs/1902.11114> (Accessed: 14 March 2024).

Nellemann, C., Corcoran, E., Duarte, C.M., Valdés, L., De Young, C., et al. (2009). Blue carbon - The role of healthy oceans in binding carbon. GRID-Arendal.

Neufeld, D., 2024. How Blue Carbon Combats Climate Change. [online] Greensponsored Post. Available at:

<https://www.visualcapitalist.com/sp/how-blue-carbon-combats-climate-change/>

[Accessed 24 January 2024].

Okus, E., Zeki, S., Demir, V., Demirel, N., Yüksek, A., Yilmaz, I. N., Yilmaz, A. A., Karhan, S. Ü. A., Müftüoglu, E., Tural, U., Murat, E., Gazioglu, C. (2010). Anchor Damage on *Posidonia oceanica* (L.) Delile Beds In The Gokova Bay. Rapp. Comm. int. Mer Médit., 39,:606.

Pansini, A., Bosch-Belmar, M., Berlino, M., Sarà, G. & Ceccherelli, G. (2022) 'Collating evidence on the restoration efforts of the seagrass *Posidonia oceanica*: current knowledge and gaps', Science of The Total Environment, 851(Part 2), 158320.

Available at: <https://doi.org/10.1016/j.scitotenv.2022.158320>. Published 10 December 2022.

Pergent, G., Bazairi, H., Bianchi, C. N., Boudouresque, C. F., Buia, M. C., Clabaut, P., Haroun, R., Harris, R. P., Reynaud, C., & Serrano, O. (2014). "Climate Change and Mediterranean Seagrass Meadows: A Synopsis for Environmental Managers." Mediterranean Marine Science, 15(2), 462-473. DOI: 10.12681/mms.621.

Pergent-Martini, C., Pergent, G., Monnier, B., Boudouresque, C.-F., Mori, C., & Valette-Sansevin, A. (2021). Contribution of *Posidonia oceanica* meadows in the context of climate change mitigation in the Mediterranean Sea. Marine Environmental Research, 165, 105236.

Piazzi, L., Acunto, S., Frau, F., Atzori, F., Cinti, M.F., Leone, L., & Ceccherelli, G. (2021). Environmental Engineering Techniques to Restore Degraded *Posidonia oceanica* Meadows. Water, 13(5), 661; <https://doi.org/10.3390/w13050661>.

- Pirc, H., 1986. Seasonal aspects of photosynthesis in *Posidonia oceanica*: Influence of depth, temperature and light intensity. Aquatic Botany, 26, pp.203-212. Available at: [https://doi.org/10.1016/0304-3770\(86\)90021-5](https://doi.org/10.1016/0304-3770(86)90021-5).
- Poursanidis, D., Traganos, D., Reinartz, P. and Chrysoulakis, N. (2019) 'On the use of Sentinel-2 for coastal habitat mapping and satellite-derived bathymetry estimation using downscaled coastal aerosol band', International Journal of Applied Earth Observation and Geoinformation, 80, pp. 58-70.
- Reynolds, P.L. (2018) 'Seagrass and Seagrass Beds', reviewed by Duffy, E. and Knowlton, N., Smithsonian National Museum of Natural History Ocean Portal. Available at: <https://ocean.si.edu/ocean-life/plants-algae/seagrass-and-seagrass-beds> [Accessed: 15 March 2024].
- Romero, J., Perez, M., Mateo, M. A., & Sala, E. (2007). The belowground organs of the Mediterranean seagrass *Posidonia oceanica* as a biogeochemical sink. Aquatic Botany, 87(2), 116-122.
- Sánchez-Lizaso, J.L., Romero, J., Ruiz, J., Gacia, E., Buceta, J.L., Invers, O., Fernández Torquemada, Y., Mas, J., Ruiz-Mateo, A. and Manzanera, M. (2008) 'Salinity tolerance of the Mediterranean seagrass *Posidonia oceanica*: recommendations to minimize the impact of brine discharges from desalination plants', Desalination, 221(1–3), pp. 602-607. Presented at the conference on Desalination and the Environment. Sponsored by the European Desalination Society and Center for Research and Technology Hellas (CERTH), Sani Resort, Halkidiki, Greece, April 22–25, 2007.
- Şener, M. and Tüfekçi, K. (2008) 'CO₂ Storage Possibilities in Karstic Regions: A Case Study from Southwestern Turkey', Energy Sources, Part A: Recovery, Utilization, and Environmental Effects, 30(19), pp. 1747-1760. doi: 10.1080/15567030701268435.

- Short, F.T., Coles, R.G. and Pergent-Martini, C., 2001. Global seagrass distribution. Global seagrass research methods, 5, p.30.
- Simpson, J., Bruce, E., Davies, K.P., & Barber, P. (2022). "A Blueprint for the Estimation of Seagrass Carbon Stock Using Remote Sensing-Enabled Proxies." *Remote Sensing*, 14(15), 3572. <https://doi.org/10.3390/rs14153572>.
- Smith, S.V. (1981) 'Marine macrophytes as a global carbon sink', *Science*, 211, pp. 838-840. doi: 10.1126/science.211.4484.838.
- Telesca, L., Belluscio, A., Criscoli, A., Ardizzone, G., Apostolaki, E. T., Fraschetti, S., Gristina, M., Knittweis, L., Martin, C. S., Pergent, G., Alagna, A., Badalamenti, F., Garofalo, G., Gerakaris, V., Pace, M. L., Pergent-Martini, C., & Salomidi, M. (2015). Seagrass meadows (*Posidonia oceanica*) distribution and trajectories of change. *Scientific Reports*, 5, 12505.
- Topouzelis, K., Makri, D., Stoupas, N., Papakonstantinou, A., & Katsanevakis, S. (2018). Seagrass mapping in Greek territorial waters using Landsat-8 satellite images. *International Journal of Applied Earth Observation and Geoinformation*, 67, 98-113.
- Traganos, D., Aggarwal, B., Poursanidis, D., Topouzelis, K., Chrysoulakis, N., & Reinartz, P. (2018). Towards Global-Scale Seagrass Mapping and Monitoring Using Sentinel-2 on Google Earth Engine: The Case Study of the Aegean and Ionian Seas. *Remote Sensing*, 10(8), 1227; <https://doi.org/10.3390/rs10081227>.
- Ünal, V., & Kizilkaya, Z. (2019). A Long and Participatory Process towards Successful Fishery Management of Gökova Bay, Turkey. Mediterranean Conservation Society.
- Vassallo, P., Paoli, C., Rovere, A., Montefalcone, M., Morri, C., & Bianchi, C.N. (2013). The value of the seagrass *Posidonia oceanica*: A natural capital assessment. *Marine Pollution Bulletin*, 75(1-2), 157-167.

Appendix:

Classification of an orthoimage on GEE:

```
// Load the orthoimage
var orthoimage = ee.Image(
    "projects/ee-urasdefne/assets/cc743463-3e58-479b-a9
50-7cd399370faa",
);
Map.addLayer(
    orthoimage,
    { bands: ["b1", "b2", "b3"], min: 0, max: 255 },
    "Orthoimage",
);

// Specify the region of interest using the image
// dimensions and origin
var region = ee.Geometry.Rectangle([
    28.0377309870714058, 36.8298397339722001,
    28.0377885369331317,
    36.8298932958475262,
]);
Map.centerObject(region, 15);

// Extract pixel size information from metadata
var pixelSizeX = 2.241911247600425631e-8;
var pixelSizeY = -1.802216531834611715e-8;

// Calculate scale based on pixel size
var scale = Math.max(pixelSizeX, pixelSizeY);

// Convert degrees to meters (approximately, as degrees
// vary with latitude)
var degreesPerPixel = 2.2419112476004256e-8;
var metersPerPixel = degreesPerPixel * 111320; // 1
// degree is approximately 111320 meters
print("Scale (meters per pixel):", metersPerPixel);

// Set threshold values for each band for seagrasses
var threshold_seagrass_b1 = 157.83;
var threshold_seagrass_b2 = 147.92;
var threshold_seagrass_b3 = 134.17;

// Set threshold values for each band for non-seagrasses
// (sand)
```

```

var threshold_sand_b1 = 197.58;
var threshold_sand_b2 = 190.19;
var threshold_sand_b3 = 180.36;

// Create binary masks for each band for seagrasses
var mask_seagrass_b1 =
    orthoimage.select("b1").gt(threshold_seagrass_b1);
var mask_seagrass_b2 =
    orthoimage.select("b2").gt(threshold_seagrass_b2);
var mask_seagrass_b3 =
    orthoimage.select("b3").gt(threshold_seagrass_b3);

// Create binary masks for each band for seagrasses
var mask_sand_b1 =
    orthoimage.select("b1").gt(threshold_sand_b1);
var mask_sand_b2 =
    orthoimage.select("b2").gt(threshold_sand_b2);
var mask_sand_b3 =
    orthoimage.select("b3").gt(threshold_sand_b3);

// Combine the binary masks into a single mask
var seagrassMask = ee
    .Image(mask_seagrass_b1, mask_seagrass_b2,
        mask_seagrass_b3)
    .reduce(ee.Reducer.allNonZero());
var sandMask = ee
    .Image(mask_sand_b1, mask_sand_b2, mask_sand_b3)
    .reduce(ee.Reducer.allNonZero());

// Display the seagrass mask
Map.addLayer(
    seagrassMask,
    { min: 0, max: 1, palette: ["000000", "00FF00"] },
    "Seagrass Mask",
);
Map.addLayer(
    sandMask,
    { min: 0, max: 1, palette: ["000000", "FFFF00"] },
    "Sand Mask",
);

```

Validation orthoimage:

```
// Load the sixth orthoimage for validation
var orthoimage6_validation =
  ee.Image('projects/ee-urasdefne/assets/7196afce-0c7
  c-4f0c-95e3-2abdd69d0d98');

// Specify the region of interest for validation
var region_validation =
  ee.Geometry.Rectangle([28.0375041858530913,
  36.8298056636676421, 28.0377384655304311,
  36.8298958465831276]);

// Center the map view on the specified region
Map.centerObject(region_validation, 15);

// Calculate the scale based on pixel size information
var pixelSizeX_validation = 2.241910787940662737e-08;
var pixelSizeY_validation = -1.802216536482223263e-08;
var scale_validation = Math.max(pixelSizeX_validation,
  pixelSizeY_validation);

// Add the validation orthoimage to the map
Map.addLayer(orthoimage6_validation, {bands: ['b1'],
  min: 0, max: 255}, 'Validation Orthoimage');

// Set threshold values for each band for seagrasses in
// orthoimage6_validation
var threshold_seagrass_b1_6 = 109.5;
var threshold_seagrass_b2_6 = 125.833;
var threshold_seagrass_b3_6 = 123.66;

// Set threshold values for each band for non-seagrasses
// (sand) in orthoimage6_validation
var threshold_sand_b1_6 = 217.0196;
var threshold_sand_b2_6 = 214.176;
var threshold_sand_b3_6 = 202.137;

// Create binary masks for each band for seagrasses in
// orthoimage6_validation
var mask_seagrass_b1_6 =
  orthoimage6_validation.select('b1').gt(threshold_se
  agrass_b1_6);
var mask_seagrass_b2_6 =
  orthoimage6_validation.select('b2').gt(threshold_se
  agrass_b2_6);
```

```

var mask_seagrass_b3_6 =
    orthoimage6_validation.select('b3').gt(threshold_seagrass_b3_6);

// Create binary masks for each band for non-seagrasses (sand) in orthoimage6_validation
var mask_sand_b1_6 =
    orthoimage6_validation.select('b1').gt(threshold_sand_b1_6);
var mask_sand_b2_6 =
    orthoimage6_validation.select('b2').gt(threshold_sand_b2_6);
var mask_sand_b3_6 =
    orthoimage6_validation.select('b3').gt(threshold_sand_b3_6);

// Combine the binary masks into a single mask
var seagrassMask_6 =
    ee.Image(mask_seagrass_b1_6).and(mask_seagrass_b2_6)
        .and(mask_seagrass_b3_6);
var sandMask_6 =
    ee.Image(mask_sand_b1_6).and(mask_sand_b2_6).and(mask_sand_b3_6);

// Display the seagrass and sand masks for orthoimage6_validation
Map.addLayer(seagrassMask_6, {min: 0, max: 1, palette:
    ['000000', '00FF00']}, 'Seagrass Mask (Orthoimage 6)');
Map.addLayer(sandMask_6, {min: 0, max: 1, palette:
    ['000000', 'FFFF00']}, 'Sand Mask (Orthoimage 6)');

```

Sentinel-2

```

// Load S-2 imagery and filter it to all images in May-August 2023.
var S2data = ee.ImageCollection('COPERNICUS/S2_SR')
    .filterDate('2023-05-01', '2023-08-01')
    .filterBounds(poi)
    .filter(ee.Filter.lt('CLOUDY_PIXEL_PERCENTAGE',
        40));
var region = poi

var count = S2data.size();

```

```

print('Number of images in the collection:', count);

// Check the band names of the first image in the
// collection
var firstImage = ee.Image(S2data.first());
print('Band names of the first image:',
      firstImage.bandNames());

// Take median
var S2composite = S2data.median();

// Create Land mask
var B8 = S2composite.select('B8');
var NIR_thres = 500;
var landmask = B8.where(B8.gt(NIR_thres),
  0).where(B8.lt(NIR_thres), 1);

// Take median of the land mask
var landmaskMedian =
  landmask.reduce(ee.Reducer.median());

// Add the median land mask to the map
var rgbVis = {min: 0, max: 3000, bands: ['B8']>;
Map.addLayer(S2composite, rgbVis, 'S2 NIR Band');
Map.addLayer(landmaskMedian.clip(poi), {palette:
  ['000000', 'FFFFFF'], opacity: 0.5}, 'Land Mask
Median');

// Export seagrasses FeatureCollection to an asset
Export.table.toAsset({
  collection: seagrass,
  description: 'seagrass_asset',
  assetId: 'users/urasdefne/path/to/seagrasses',
});

// Export sand FeatureCollection to an asset
Export.table.toAsset({
  collection: sand,
  description: 'sand_asset',
  assetId: 'users/urasdefne/path/to/sand',
});

// Classification

// Training data
var seagrass =
  ee.FeatureCollection('users/urasdefne/seagrass');
var sand = ee.FeatureCollection('users/urasdefne/sand');
var trainingPolygons = seagrass.merge(sand);

```

```

// Define the bands to use for classification
var bands = ['B2', 'B3', 'B4', 'B8'];

// Print the band names of the Sentinel-2 image
print('Band names:', S2composite.bandNames());

// Sample the Sentinel-2 image at the locations of
// training data
var training = S2composite.select(bands).sampleRegions({
  collection: trainingPolygons,
  properties: ['class'],
  scale: 10
});

// Print the first feature to check if it has the
// sampled bands
print('First sampled feature:', training.first());

// Train a Random Forest classifier
var classifier = ee.Classifier.smileRandomForest({
  numberOfTrees: 10,
  minLeafPopulation: 1
}).train({
  features: training,
  classProperty: 'class',
  inputProperties: bands
});

// Classify the Sentinel-2 image
var classified =
  S2composite.select(bands).classify(classifier);

// Mask out non-coastal areas using the land mask
var landmaskClipped = landmask.clip(poi).eq(1);
var classifiedMasked =
  classified.updateMask(landmaskClipped);

// Add the masked classification to the map with an
// improved color palette
Map.centerObject(poi, 10);
Map.addLayer(classifiedMasked, {
  min: 0,
  max: 2,
  palette: ['00FF00', 'FF0000'], // Blue for sand,
  // Green for seagrass, Red for unclassified
}, 'Seagrass and Sand Classification (Coastal Only)');
Map.addLayer(poi, {}, 'POI');

// Display the map

```

```

Map;

// Classify the Sentinel-2 image
var classified =
    S2composite.select(bands).classify(classifier);

// Add the classified image to the map with an improved
// color palette
Map.centerObject(poi, 10);
Map.addLayer(classified, {
    min: 0,
    max: 2,
    palette: ['0000FF', '00FF00', 'FF0000'], // Blue for
        sand, Green for seagrass, Red for unclassified
}, 'Seagrass and Sand Classification');
Map.addLayer(poi, {}, 'POI');

// Display the map
Map;

// Print and inspect the classified image to see the
// pixel values and identify any patterns or issues
print('Number of features in seagrass:',
    seagrass.size());
print('Number of features in sand:', sand.size());
print('Training Data:', trainingPolygons);
print('Classifier:', classifier);
print('Classified Image:', classified);
var landmask = B8.where(B8.gt(NIR_thres),
    0).where(B8.lt(NIR_thres), 1);

// Inspect Training Data Properties
var firstTrainingFeature = trainingPolygons.first();
print('Training Feature Properties:',
    firstTrainingFeature);

// Class distribution
var classDistribution = classified.reduceRegion({
    reducer: ee.Reducer.frequencyHistogram(),
    geometry: poi,
    scale: 10,
});

print('Class distribution:',
    classDistribution.get('classification'));

// Set a threshold to convert continuous values to
// binary (e.g., 1 if value > threshold, else 0)
var threshold = 1;

```

```

var binaryClassification = classified.gt(1);

// Add the binary classification map to the map
Map.addLayer(binaryClassification, {
  min: 0,
  max: 1,
  palette: ['0000FF', '00FF00'], // Blue for class 0,
  Green for class 1
}, 'Binary Seagrass and Sand Classification');

// Splitting the datasets for training and validation
var split = 0.7; // 70% for training, 30% for validation
var seagrassSplit =
  seagrass.randomColumn().filter(ee.Filter.lt('random',
    split));
var sandSplit =
  sand.randomColumn().filter(ee.Filter.lt('random',
    split));

// Assuming 'seagrass' and 'sand' are your reference
// data
var validationData =
  seagrass.merge(sand).filter(ee.Filter.gte('random',
    split));

// Get validation accuracy
var validated = validationData.classify(classifier);
var errorMatrix =
  validated.errorMatrix('classification',
    'classification'); // Use 'classification' for both
  actual and predicted class labels
print('Error Matrix', errorMatrix);
print('Accuracy', errorMatrix.accuracy());

```